DIELECTRIC RESONATOR AND MULTI-LAYERED REFLECTARRAYS

WONG HONG YIK

MASTER OF ENGINEERING SCIENCE

Faculty of Engineering and Science

Universiti Tunku Abdul Rahman

DECEMBER 2014

ABSTRACT

A reflectarray is an array of radiating elements that give a pre-designed phasing to produce a directional beam when it is illuminated by a feed antenna, similar to a parabolic reflector. Meanwhile, it possesses some of the salient advantages of both the reflector and phased array. It is broadly used to steer reflection beams to the desired directions as in a phased array. On the other hand, reflectarray uses the feeding method as in a reflector antenna thus eliminates the use of complex and higher loss feeding network. When the waves coming from feed horn impinge on a reflectarray, each resonating unit imposes a certain phase shift to the reflected signal and forms a planar reflection phase front. As a result, the main beam can be switched to different directions by controlling the phase shifts of all the elements.

Varying the resonator size and adding loading element are among the most common techniques used to provide phase shift in the design of a reflectarray. Prior to the design of reflectarray, infinite periodic array approach was used to simulate the single resonator element in order to examine the reflection phase characteristics of the element under the mutual influences of an infinitely large array environment. In this thesis, several reflectarrays with different types of radiating elements have been introduced. My work can be divided into two parts. Radiating elements such as dielectric resonator (DR), circular and elliptical microstrip patches have been selected to demonstrate the design ideas.

ACKNOWLEDGEMENT

I would like to express my sincere appreciation to Dr. Lim Eng Hock for his guidance, ideas and editing of this dissertation. Throughout the completion of this research project, a lot of invaluable recommendations and suggestions have been shared. In addition, he was always available whenever I faced doubt.

I also wish to thank Mr. Ho and Mr. Tham, who guided me on solving the problems that I faced during the fabrication process. With their experience, I am able to fabricate my design smoothly. Besides that, I also like to extend my gratitude to my course mates for their assists during the experiment.

Special thanks should be given to UTAR for providing all the equipments, facilities, and materials. Furthermore, the online database such as IEEE Xplore and ProQuest are very handy where most of the important literatures are available.

APPROVAL SHEET

This dissertation entitled **'DIELECTRIC RESONATOR AND MULTI-LAYERED REFLECTARRAYS'** was prepared by WONG HONG YIK and submitted as partial fulfillment of the requirement for the degree of Master of Engineering Science at Universiti Tunku Abdul Rahman.

Approved by,

_____

(Dr. Lim Eng Hock) Date: _____

Supervisor

Department of Electrical and Electronic Engineering

Faculty of Engineering Science

Universiti Tunku Abdul Rahman

FACULTY OF ENGINEERING SCIENCE

UNIVERSITI TUNKU ABDUL RAHMAN

Date: 17th December 2014

SUBMISSION OF DISSERTATION

It is hereby certified that **WONG HONG YIK** (ID No: **09 UEM 09094**) has completed this dissertation entitled "**DIELECTRIC RESONATOR AND MULTI-LAYERED REFLECTARRAYS**" under the supervision of Dr. Lim Eng Hock (Supervisor) from the Department of Electrical and Electronic Engineering, Faculty of Engineering and Science (FES)

I understand that University will upload softcopy of my final dissertation in pdf format into UTAR Institutional Repository, which may be made accessible to UTAR community and public.

Yours truly,

_____

(WONG HONG YIK)

DECLARATION

I hereby declare that the dissertation is based on my original work except for citations and quotations which have been duly acknowledged. I also declare that it has not been previously and concurrently submitted for any other degree or award at UTAR or other institutions.

Name : WONG HONG YIK

Date : 17th December 2014

DIELECTRIC RESONATOR AND MULTI-LAYERED REFLECTARRAYS

In the first part, the feasibility of using DRs as radiating element is explored for a newly proposed reflectarray. It has been shown that the bottom-loading variable length rectangular strip on a rectangular DR can introduce a certain degree of phase shift to the reflected signal. The loss of a DR is usually lower than that for a metallic patch because of the absence of conductive loss, especially in the millimeter-wave ranges. In this design, the strip is directly made by the standard PCB etching process. By directly etching the strip on a substrate, a more accurate strip dimension can be obtained.

In the second part, the multilayer substrate concept has been introduced for designing different reflectarrays. In the first case, circular microstrip patches of different radiuses are deployed as the radiating element. To demonstrate the design idea, the resonator is made on a double-layered foam-backed substrate. Foam is one of the most frequently used low-cost materials. Tuning the foam thickness can provide an additional degree of design freedom, leading to different phase variation curves with varied slopes and dynamic phase ranges. It has also been found that this reflectarray element has a wide dynamic range of phase shift with less sensitivity. This can facilitate the design process greatly. To further improve the bandwidth performance, subsequently, the elliptical patch is used as a resonator. It was found that a much broader antenna bandwidth, comparing with that for circular patch, is achievable by changing the major-to-minor ratio of the

elliptical patch. Both of the reflectarrays are designed to work in the frequency range of 5.5GHz – 7.5GHz with a center design frequency of 6.5GHz.

In this dissertation, as can be seen, different new reflectarrays have been proposed and studied. Infinite periodic array method is successfully used to design the reflectarrays. Finally, experiments have been carried out to verify the theoretical findings.

TABLE OF CONTENTS

LIST OF TABLES

LIST OF FIGURES

CHAPTER 1

BACKGROUND AND INTRODUCTION

1.1 Background and Issues

Parabolic reflectors and phased arrays are the primary choices for the conventional wireless applications that require high gain. The parabolic disc of the reflector antenna is a powerful tool to focus microwave signals into a certain direction. Fabricating such curved surface, however, can be very challenging and expensive (Zhou, M. et al., 2013). Also, the disc is usually made of some metallic materials, making it very bulky (Huang, J., 1995). This may not be ideal for space-borne applications as space and weight are among the scarcest resources. To enable signal transmission and reception in different directions, mechanical rotator is usually incorporated with a reflector antenna to change the direction of the radiation aperture, making it very inconvenient. Electronically controller phased array, which is made by combining multiple antennas into array form with each of them having a different input phase, is obviously a good solution as it enables beam scanning. However, the phased array requires a phase-shifting power dividing network to supply different phases to its individual elements. Such feeding network can be complicated, expensive, and causing higher loss.

Reflectarray is one type of new antenna that combines some of the good features of both the conventional reflector antenna and the phased array

(Mener, S. et al., 2013), with some of the drawbacks tackled (Mussetta, M. et al., 2007). It was first proposed by Berry et al. (Berry, D. et al., 1963) in 1963. The most attractive feature of the reflectarray is its flat and compact reflecting surface that makes it relatively easy to make comparing with a curved parabolic reflector (Huang, J., 1996). It is also lighter and has a lower profile than the reflector needing less supporting fixtures. That makes it very popular for the space-borne structures such as satellite or spacecraft. Since all the radiating elements of a reflectarray are spatially excited by a feed antenna, unlike phased array, it does not need any power dividing network (Pan, Y. et al., 2012) to feed its individual radiating element. The antenna gain of the reflectarray can be enhanced by increasing the radiation aperture which enables the reflecting surface to host more radiating elements.

The working principle of the reflectarray is now discussed. It consists of a planar reflector and a feed antenna as shown in Figure 1.1. Like the parabolic reflector antenna, the planar reflecting surface of the reflectarray is spatially illuminated by a feed antenna. The reflecting surface (Biallowski M. E. and Encinar, J., 2007) can be either circular or square in shape. An incident angle θ that varies from 0^o to 40^o is applied (Huang J. and Encinar, J. A., 2007). If the planar reflector is a piece of metal, the wave beams end up with varied wave fronts as they have travelled different distances. For a typical reflectarray, shown in Figure 1.2, the reflecting surface usually consists of multiple radiating elements, which are placed on a grounded substrate. The array of radiating elements is designed in the way that each is adding the incident wave beam with a certain phase shift such that the reflected wave

beams can have an identical wave front along the line *A – A'* (Zhang, W. X. et al., 2007), making it to form a directional radiation beam in a particular direction (Boccia, L. et al., 2002). The propagating direction of this wave front determines where the main lobe of the reflectarray is pointing to. In other words, the reflectarray is responsible to transform the spherical wave front of the feed antenna into a planar one (Bialkowski M. E. and Sayidmarie, K. H., 2008), as shown in Figure 1.2 and the transformation is achieved by introducing different phase shifts to all the radiating elements (Venneri, F. et al., 2013).

The feeding path of each element is of different length, causing the reflection phase of each to be different. Based on these differences, the phase shift that is required by each of the radiating elements can then be calculated. With reference to Figure 1.2, the phase of each wave beam can be calculated along the reference line *A – A'*. A minor phase shift is then introduced to each element so that the phases of all rays can be made identical along the reference. Usually, this can be done by varying one of the geometrical design parameters of the radiating element. It is crucial that any change on this parameter can be translated into a certain variation in the reflection phase (Nayeri, P. et al., 2013).

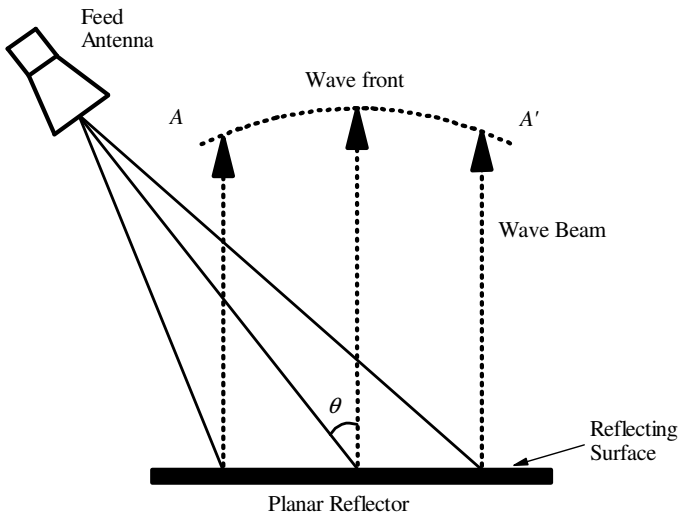

Figure 1.1: The configuration of a reflectarray which consists of a planar reflector and a feed antenna.

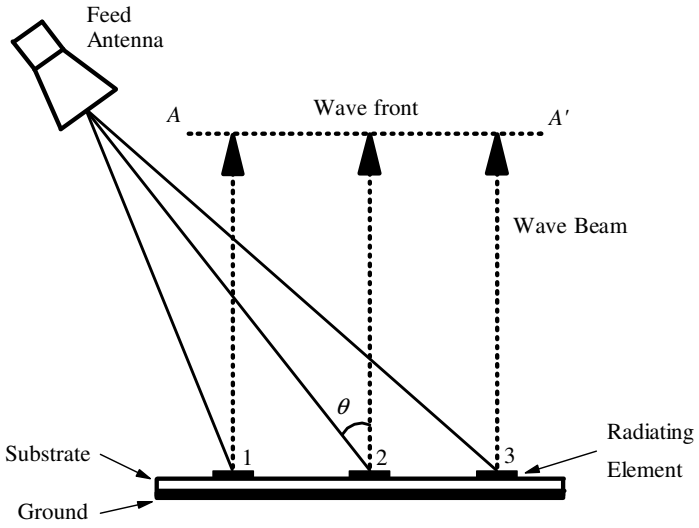

Figure 1.2: A typical reflectarray with multiple wave beams reflected by the radiating elements. Each element is pre-designed to radiate with a different phase shift so that all beams will have the same wave front along $A - A'$.

Figure 1.3 shows two typical methods which can be used to shift the reflection phase of a single radiating element. In this case, a conventional microstrip patch has been deployed. The first one is depicted in Figure 1.3 (a) where patches with variable sizes are used to achieve different phase shifts in the radiating elements (Pozar D. M. and Metzler, T. A., 1993; Pozar, D. M. et al., 1997). In other words, the microstrip patch with a certain size will slap a fixed amount of phase shift to an incident wave, resulting in a reflected wave that is compensated. For the second method shown in Figure 1.3 (b), the square microstrip patches are loaded with stubs with variable lengths, which are used as the phase shifters (Huang, J., 1991; Chang D. C. and Huang, M. C., 1995; Bialkowski, M. E. et al., 2001) Here, the phase shifting mechanism is achieved by varying the length of the phase-delaying stub line attached to the patch (Javor, R. D., 1995). For both, any change in the geometrical design parameter causes the input impedance to vary, making the reflection phase to be different. Printed microstrip patches, dipoles (Pozar, D. M. et al., 1999), and rings are among the popular choices for designing the reflectarray

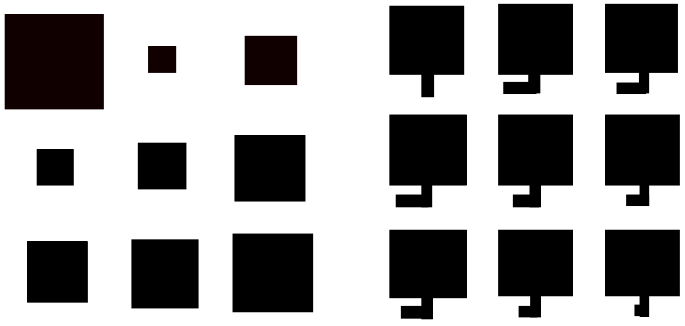

(a) (b)

Figure 1.3: Two typical radiating elements with different geometrical parameters for shifting the reflection phase: (a) Patches with variable size. (b) Identical patches with variable phase-delaying stub.

There are two types of feeding schemes commonly used by various reflectarrays – center-fed ($\theta = 0^o$) and side-fed or offset fed, ($\theta > 0^o$). The former has the feed antenna located right above the centre point of the reflecting surface that is used to accommodate the radiating elements. What the most undesirable here is that the feeder is blocking the radiation beam. This is because the feed antenna is made from conductive metal which can scatter the reflected wave from the reflectarray. It degrades the reflectarray performance, primarily the antenna gain and the radiation pattern (Almajali, E. et al., 2012). This can be solved by re-locating the feed antenna, making it to have a particular illumination angle (θ) from the center axis (Abd-Elhady, M. and Wei Hong, 2010), as shown in Figure 1.2. A side-fed configuration can avoid the blockage of the broadside radiation beam by the feed antenna itself (Han, C. et al., 2006; Mussetta, M. et al., 2006; Yang, F. et al., 2007; Yu, A. et al., 2009; Budhu J. and Rahmat-Samii, Y., 2011; Abd-Elhady, A. M. et al., 2012). Usually, the feed antenna is a horn but it also can be a dipole (Milon, M. et al., 2006).

1.2 Key Performance Parameters

In this section, some of the yield sticks for the reflectarray are discussed. To be a good antenna, a reflectarray is required to give broad bandwidth and high antenna gain. Of course, the antenna performance will only be good if each of the individual reflectarray elements can be made to have the optimized reflection characteristics.

1.2.1 Unit Element

The reflection coefficient of a reflectarray element can be extracted from the unit cell simulation by using either the Waveguide Method or Floquet Method, which will be described in Chapter 2. A port is set up at a distance from the radiating element to emulate plane wave impingement.

1.2.1.1 Reflection Loss

When a reflectarray element is reflecting the incoming wave, some losses will be introduced by the element itself. They are primarily comprised by metallic ohmic loss and dielectric loss (Bozzi, M. et al., 2004). The loss tangent and thickness of a substrate can affect the reflection characteristics significantly (Rajagopalan H. and Rahmat-Samii, Y., 2010). It is reported by (Bozzi, M. et al., 2004) that the amount of reflection loss is also affected by the shape of the radiating element. The information of the reflection loss can

be extracted from the magnitude of the reflection coefficient in the unit cell simulation at a particular frequency. Unlike the return loss of the conventional antenna, the reflection loss of a reflectarray element should be minimized.

1.2.1.2 Phase Range and Slope

Another important result that has to be extracted from the reflection coefficient is phase. The relationship between the reflection phase with the phase-shifting design parameter (Niaz, M. W. et al., 2010), such as the width, length or height of a reflectarray element, is defined as the S-Curve, or simply referred as reflection phase by some publications. By knowing the additional phases that are required by all elements (Hasani, H. et al., 2010), the S-Curve can be used to design the dimensions of all the radiating elements of a reflectarray. Full elaboration will be given in Chapter 2-4. The changing rate (gradient) of the S-Curve tells how sensitive the reflection phase is corresponding to variation of the phase-shifting design parameter. Slow gradient is usually better as the dimensions of the radiating elements can be made more distinguished. Also, the range of the phase change has to be large enough for designing all element of the reflectarray.

It was found that the phase range is related to the element spacing, which is defined as the inter-element centre-to-centre distance between the adjacent radiating elements (Karnati, K. et al., 2010). Different element spacing causes the S-Curve to be different due to effect of mutual coupling (Karnati, K. et al., 2013). Conventionally, an element spacing of around 0.5λ

at the centre design frequency is expected to produce an S curve with suitable phase slope and sufficient phase dynamic range. It was reported in (Robinson, A. W. et al., 1999) that an overly large element spacing (> 1λ) can cause undesired side lobes in the radiation pattern of reflectarray. The slope of S-Curve can be reduced (Hasani, H. et al., 2010) with the use of thick substrate (Karnati, K. et al., 2011), stacked patches (Encinar, J. A., 1999; Encinar, J. A., 2001), phase delay line (Carrasco, E. et al., 2008) and etc.

1.2.2 Reflectarray

The radiating elements of a reflectarray are to convert the spherical wave front emitted from the feed horn into a plane wave. Since the distances of the radiating elements from the feed horn are different (Robinson, A. W. et al., 1999; Makdissy, T. et al., 2012; Mussetta, M. et al., 2012), all the elements have to be able to compensate the wave beams from different path lengths at once, making them to be in-phase (Adel S. and Hammad, H., 2013) before the reflectarray aperture. An in-phase reflected wave front will form a directive radiation beam due to constructive interference of the all the wave rays (Karnati, K. et al., 2013). The performance of the reflectarray is affected by the reflection characteristics of the individual element as well as the inter-element spacing.

1.2.2.1 Antenna Gain

A reflectarray is to generate highly directive antenna gain that is comparable to that of the parabolic reflector and phased array. Because the reflectarray is usually built by passive components, its antenna gain is primarily affected by the aperture size (Huang J. and Encinar, J. A., 2007). More elements in a reflectarray can bring about a higher antenna gain. It was found that the spill-over losses can be mitigated by placing the feed horn nearer to the aperture, resulting in a better antenna gain. As a reflectarray is designed from the S-curve generated at a certain incident angle, the feed horn has to be configured in this angular setting for an optimized antenna gain.

1.2.2.2 Gain Bandwidth

Gain bandwidth is another important performance parameter of a reflectarray describing the frequency range in which the gain drop is less than 1 dB (or 3 dB), which is mainly limited by the bandwidth of the single element (Huang J. and Encinar, J. A., 2007). The main shortcoming of a microstrip reflectarray is its narrow bandwidth performance as microstrip resonator has narrow bandwidth. It is reported in (Encinar, J. A., 1999; Encinar J. A. and Zornoza, J. A., 2003) that the bandwidth of a microstrip reflectarray can be improved with the use of thicker substrate and stacked patches.

1.3 Objectives and Motivations

The aim of this research is to apply novel ideas on designing the DRA and microstrip-based reflectarrays. The first part of this thesis is dedicated to the exploration of the DRA reflectarray. Later, the circular and elliptical patches made on the multilayered substrate are studied. The design method, modeling, simulation, and experimental verification have been presented to verify the performances of the proposed new reflectarrays, with the details described in the following paragraphs.

For the first time in Chapter 3, an under-loading strip is used as the phase shifter of the dielectric resonator antenna. The length of the strip is varied for obtaining changeable phase shift. It is found that a dynamic range of 336^{o} is achievable. To demonstrate the design idea, a total of 49 glass elements are used to design a 7×7 DRA reflectarray, working at 6.5 GHz. Experiment was carried out to verify the simulated result. Parametric analysis was performed on some of the design parameters to find out their effects.

In Chapter 4, also for the first time, a novel elliptical microstrip patch is used in the design of reflectarray. A 9×9 elliptical patch reflectarray was design for this case. In order to shift the reflection phase, the major axis of the elliptical patch is varied. For comparison, a similar circular patch reflectarray has also been designed. Since the elliptical microstrip patch resonator has a broader antenna bandwidth than the circular one, it is the motivation here to

translate this feature into the gain bandwidth of the reflectarray. To increase the range of the changeable phase shift of the single radiating element, foam board has been incorporated into the microstrip substrate to form a multilayer structure.

1.4 Thesis Overview

In Chapter 1, the design concept of the reflectarray is discussed, along with a review on the background. Explanations on some of the key performance parameters are presented. Finally, the motivation and objectives of this research are ensued.

Chapter 2 describes the design methodology of reflectarray. This includes the simulation and modeling of the single radiating element. Also given is the design procedure for the reflectarray. Different modeling methods have been also discussed.

Chapter 3 presents the design of the DRA reflectarray with a bottom-loading rectangular strip. Details of the design, fabrication and testing of the DRA reflectarray are included, along with the simulation and measurement results. Parametric analysis is performed for the key design parameters of the DRA reflectarray.

Chapter 4 focuses on the design of two microstrip reflectarrays. The design, fabrication, and testing processes of the circular and elliptical patch

reflectarrays are described. Simulation and measurement results together with other findings are also presented.

Chapter 5 summarizes the work completed in this thesis. Discussion on the key findings of this research is included.

CHAPTER 2

DESIGN METHODOLOGY

2.1 Review of Design Methods

There are two types of design methods used for the design of the reflectarray. The first method goes with the use of generalized direct optimization technique (GDOT) and second one comes with phase-only synthesis. The GDOT employs the Spectral-domain Method of Moments (SDMoM) which is usually used for designing the reflectarray that involves arbitrarily-shaped elements with irregular orientations and positions. Since the locations of all the elements for this type of reflectarray are not arranged in square grid, it is impractical to calculate the reflection phase of each element. An example is that demonstrated in (Zhou, M. et al., 2013). Such method is time consuming because the computer needs to simulate, analyze, and optimize all the possible combinations in arranging the elements, which may consume much computational resources. As a result, the more popular approach for designing a reflectarray is the phase-only synthesis technique (Encinar, J. A. et al., 2006). The number of phase-shifting elements is first determined in this technique; the wave propagation phases for all other elements are then compared with a selected referencing element for the calculation of the compensating phase shifts (Zhou, M. et al., 2013). The phase-only synthesis technique is more direct and definitive, avoiding the necessity of running numerous computer simulations before obtaining a

workable prototype. Many reflectarrays which are designed with this technique have been demonstrated (Encinar J. A. et al., 2004; Arrebola, M. et al., 2006; Carrasco, E. et al., 2007; Capozzoli, A. et al., 2007; Carrasco, E. et al., 2008; Arrebola, M. et al., 2009; Capozzoli, A. et al., 2009; Capozzoli, A. et al., 2010; Encinar, J. A. et al., 2011; Capozzoli, A. et al., 2012).

The phase-only synthesis technique is adopted in this thesis. Figure 2.1 shows the design procedure in the flowchart form. It starts with the simulation of a single resonator in which the reflection phase for each reflectarray element is obtained by applying an oblique incident wave. The phase-shifting parameter of the element is first identified and it is varied to study the behaviour of its reflection phase. The phases for all dimensions are then combined up for the plot of the variation curve (S curve). This curve will later be used for obtaining the compensating phase for each element in the reflectarray. With the configuration of the reflectarray determined, the next step is to calculate the path lengths that are travelled by the feeding wave beams coming from a horn placed at a fixed distance with a constant inclination. By knowing the operating frequency, the propagation phase for each of the path length can be calculated. By taking one of the unit elements as reference, usually the nearest, the phase difference of another element located at a certain position can then be calculated. This difference is corresponds to the phase shift that is needed by each of the element. Then element dimensions are then directly extracted from the aforementioned S-Curve. A planar wave front can be formed in the boresight direction of the reflectarray of all the wave beams have been properly compensated by all the elements. With the

dimensions of all the elements determined, the model is then constructed using the CST Microwave Studio for simulation. Finally, the prototype will be fabricated and the performance will be verified. In the following sections of this chapter, each step of the design process shown in Figure 2.1 will be explained in detail.

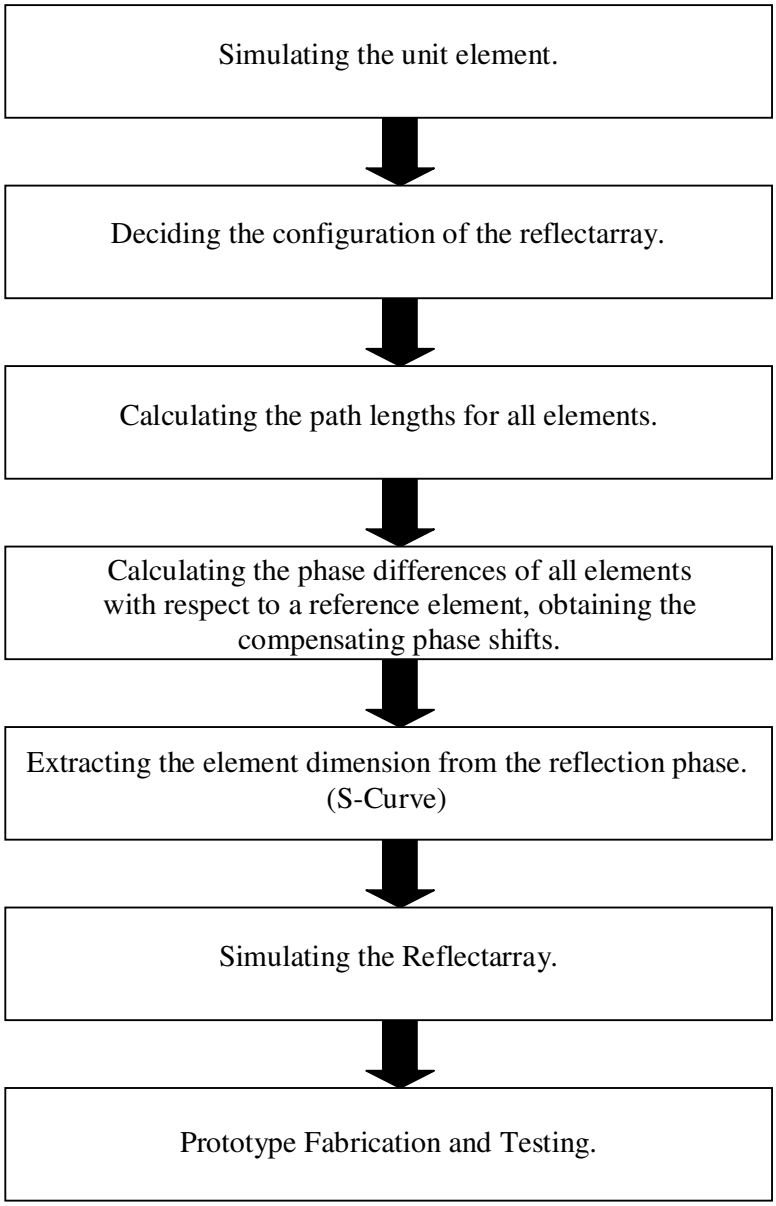

Figure 2.1: Design procedure of a reflectarray antenna using the phase-only synthesis technique.

2.2 Unit Element Simulation

The objective of the unit element simulation is to understand the change of reflection loss and phase with respect to the phase-shifting parameter of the element. Of course, first of all, it is very crucial to identify a design parameter of the element that can give enough phase changing range when the parameter is varied. Waveguide Method and Floquet Port Method are among the popular methods commonly used for performing this modelling. Both the Ansoft HFSS and CST Microwave Studio have provided computational simulators that can be used to perform such calculations, which will exemplified in the following subsections.

2.2.1 Waveguide Method

The simulation model places the unit element at one end of a rectangular waveguide (dimension: $a \times b \times l$) to receive the incident wave, operating at TE_{10} mode, coming from the waveguide port located at another, as shown in Figure 2.2. With reference to the figure, the incident angle (α) can be calculated as

$$\alpha = 90^o - \cos^{-1}\sqrt{1-(\frac{f_c}{f})^2} \quad . \qquad (1)$$

To demonstrate, a C-band rectangular waveguide (5.85GHz – 8.20GHz), with dimension a = 34.85 mm, b = 15.8 mm, l = 154 mm, is used in the model. Since the frequency of interest is taken to be 6GHz, which is equivalent to an incident angle of 44.21°, as can be calculated by eqn. (1). The unit element

here is a DRA (ε_r = 7, tan δ = 0.01, L_d = 14 mm and H_d = 6mm) that is attached with a top-loading metallic strip (L_s = 13 mm and W_s = 2 mm). The DRA is placed at the center of the ground plane. In this case, no substrate is used and the DRA is directly placed on a ground plane. It is found that inclining the strip angle (θ) can cause the incident wave to scatter with different phase; therefore, it is used as the phase shifter for the reflectarray. The commercial software CST Microwave Studio is used to simulate the model. A waveguide section and a SMA-to-waveguide adaptor, shown in Figure 2.3, are deployed for measuring the reflection characteristics. In the experiment, a sticky copper tape is cut and stuck on top of the DRA. The reflection coefficient can be measured through the SMA connector, and the reflection magnitude and phase are then extracted for plotting the reflection loss and S-Curve. Figure 2.4 shows the simulated and measured reflection loss and S-Curve. The loss peaks at -0.4 dB at the inclined angle of $\theta = 25^{o}$. This is because the resonant frequency of the strip-loaded DRA is around 6 GHz, causing more energy consumption. Also depicted in the figure is the S-Curve. The total phase shift introducible by the strip rotation is measured 162.29^{o} (simulation 147.01^{o}), which is not sufficient for a large reflectarray, which usually needs a phase range of around 360^{o}. In Waveguide Method, simulation of square cell is not possible because the size of the unit cell has to follow the waveguide dimension ($a \times b$). This slaps limitation on the spacing between the reflectarray elements. It will be shown later that an element spacing of 0.5λ - 0.6λ is the most desired for achieving the maximum phase-shifting range in each element in the patch reflectarray, but this distance is usually not possible here.

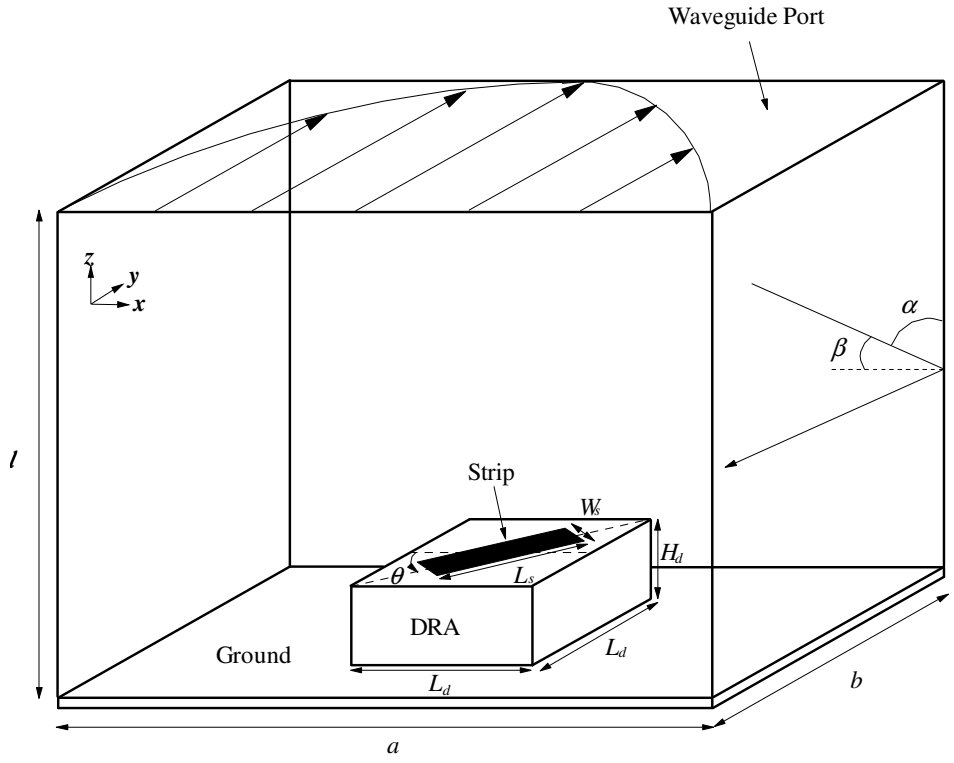

Figure 2.2 The unit cell for a DRA top-loaded with an inclined metallic strip (L_s = 13mm, W_s = 2mm, $0° \leq \theta \leq 90°$, L_d = 14mm, H_d = 6mm, a = 34.85 mm, b = 15.8 mm, l = 154 mm).

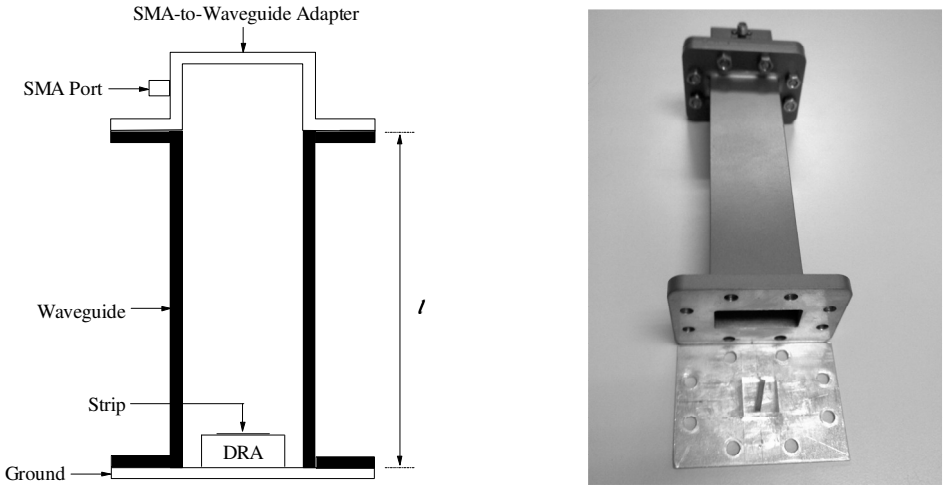

(a) (b)

Figure 2.3 Experimental setup for the waveguide method. (a) Cross-sectional view. (b) Photograph.

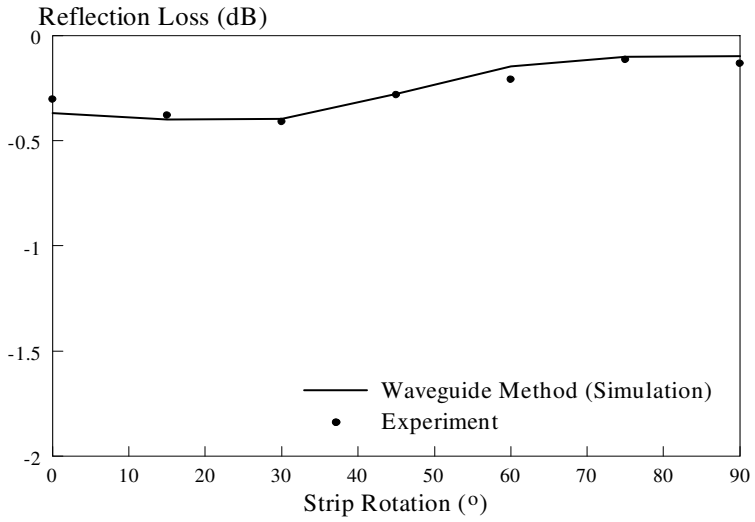

(a)

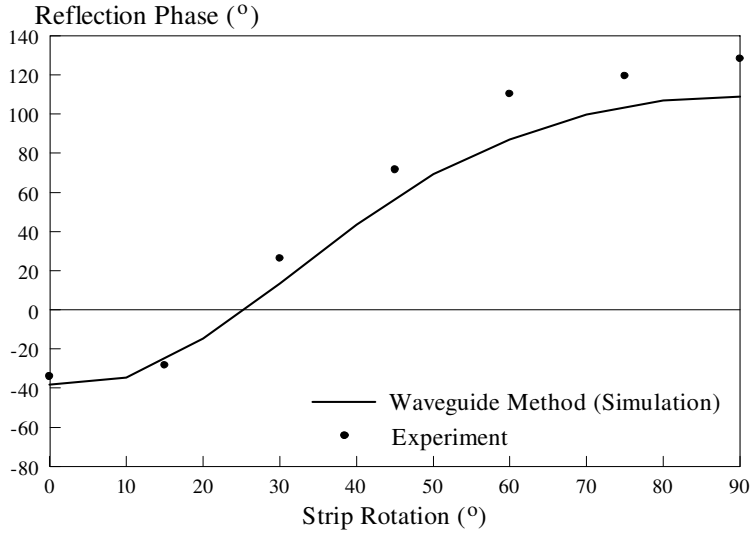

(b)

Figure 2.4 Simulated and measured (a) reflection loss and, (b) S-Curve at 6GHz.

2.2.2 Floquet Method

Next, the same DRA element will be simulated by using Floquet Method. Figure 2.5 shows the simulation model. The Floquet Method provides the periodic boundary condition so that the element can be virtually extended into an infinite array considering mutual coupling among the elements, making the simulation more accurate. The incident angle of the incident wave does not depend on the frequency. This gives much freedom as the incident angle and operating frequency can be chosen freely in this design method. Most importantly, there is no limitation in selecting the spacing between the resonating elements by controlling the cell size ($L_1 \times L_2$). To simply the reflectarray design, square cell $L_1 = L_2$ is used. The simulated S-Curves for different element spacings are given in Figure 2.6. For square cases ($L_1 = L_2$), it can be seen that the changeable range increases when the spacing becomes less. The distance between the Floquet port and the resonating element is not important as the port can be de-embedded close to the element surface at the end. More examples on Floquet Method will be given in Chapters 3 and 4.

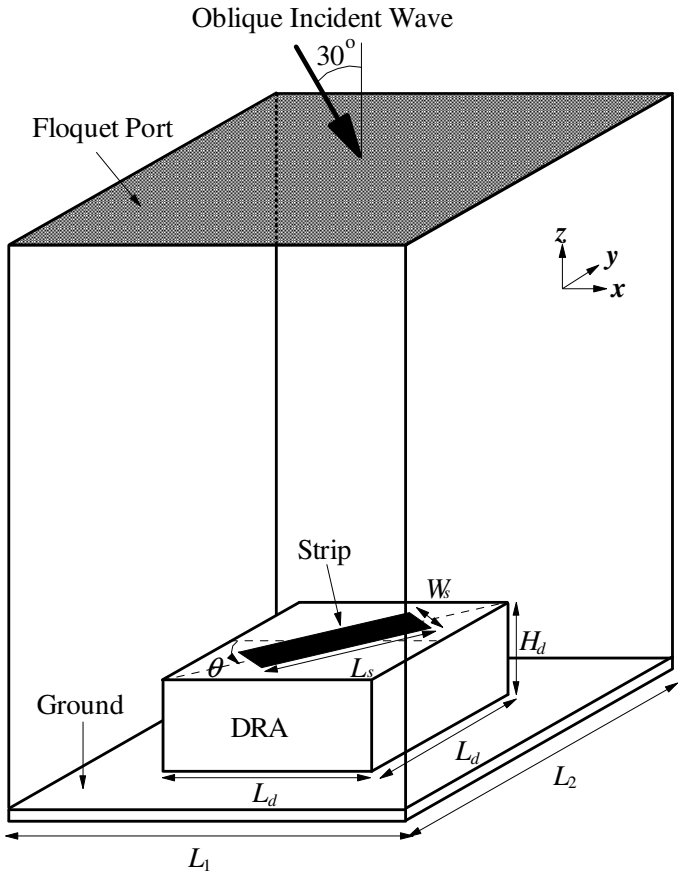

Figure 2.5 The Floquet cell for a DRA top-loaded with an inclined metallic strip.

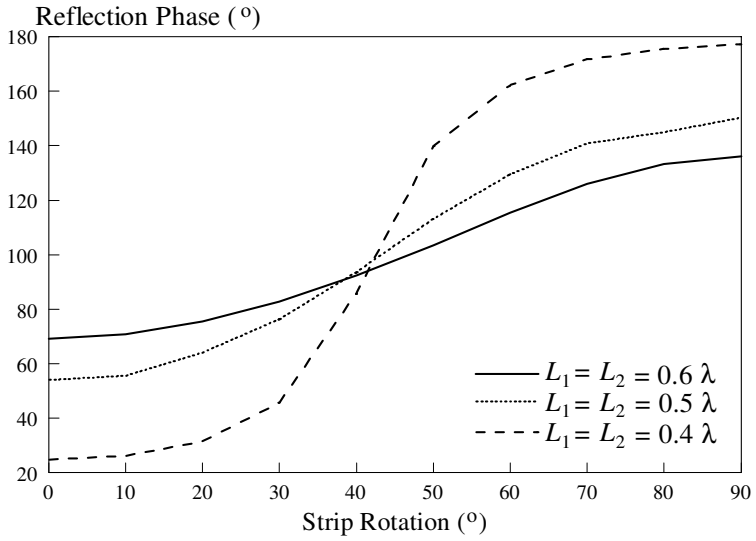

Figure 2.6 Simulated S-Curves of the strip-loaded DRA with several different element spacing ($L_1 = L_2$).

For both the unit cell simulations, Ansoft HFSS offers a much more convenient solution as the reflection phase variation curve (S-Curve) of a reflectarray element can be easily obtained without additional post-processing steps. In CST simulation, extra steps are always needed to extract the S-Curve. It involves the simulation of reflection coefficient (magnitude and phase) in each case of varied dimension. Then, the reflection loss and S-Curve can be extracted by using a post processor.

2.3 Reflectarray Configuration

Design parameters such as the array size and the feeder position have to be determined before designing a reflectarray. Figure 2.7 shows the side view of a reflectarray. The number of elements in a reflectarray decides the antenna gain. More elements with proper spacing result in a larger gain. The feed antenna is usually a horn suspended at a focal distance *f* from the center point of the radiation aperture, which can be made in center- or side-fed configuration. All the reflectarray elements must be located in the far-field distance of the horn. The side-fed feeder is usually more favourable since the feeder itself does not block the main beam of the reflectarray. The distance *f* is also associated with the aperture dimension (*D*) of the reflectarray. The typical *f/D* ratio is usually around *f/D* = 1 (Venneri, F. et al., 2008; Zhao, M.-Y. et al., 2013).

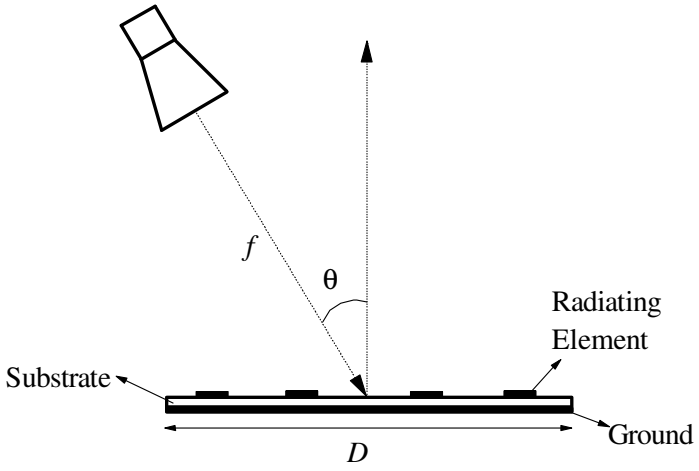

Figure 2.7: Configuration of a reflectarray.

2.4 Path Length Calculation

Figure 2.8 illustrates the propagation paths between the feed horn and the all the reflectarray elements, labelled as P_1, P_2, P_3, … , P_n. describable in millimeter. By knowing the position of the feed horn and the location of a certain element, the path length of the propagating wave from the feeder to that particular element can be calculated, which is equal to a propagation phase at a fixed frequency. Since the distances from all the elements to the feed horn are different, the path lengths $P_1 \neq P_2 \neq P_3 \ldots \neq P_n$. Detailed elaboration will be shown in Chapter 3 and 4.

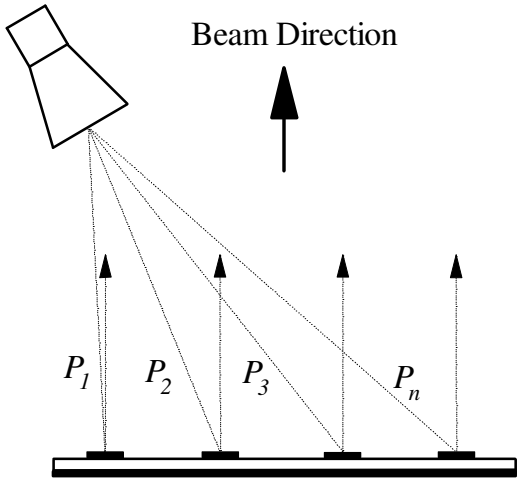

Figure 2.8: Path lengths of all the radiating elements from the feed horn.

2.5 Phase Difference Calculation

By taking one of the radiating elements to be the referencing point, the propagation phase differences between this reference and other elements can be easily calculated. As an instance, if P_1 path is taken to be the reference, the phase difference between the n-th element and this reference is $\frac{2\pi(P_n - P_1)}{\lambda_o}$, where λ_o is the wavelength at the design frequency of the reflectarray. This phase difference is the additional phase that is needed by the n-element to make it possess the same propagation phase as the reference element. By compensating the propagation phases of all elements, a planar reflection phase front can be formed before the radiation aperture of the reflectarray.

2.6 Extraction of Phase-shifting Dimension

By knowing the phase difference, the corresponding element dimension that is required by each radiating element can then be found out from the S-Curve. Although only the effect of top-loading strip was discussed for the rectangular DRA in Section 2.2, other types of reflectarrays may require phase-shifting mechanism such as varying the patch radius, dipole length, DRA height and etc.

2.7 Reflectarray Simulation

The commercially available software CST Microwave Studio is used in this case as its time-domain simulator allows the simulation of the electrically large objects such as reflectarray. A CST simulation model is constructed from the calculated element dimensions as mentioned in Section 2.6. Also included in the simulation is the feed horn, which is drawn according to the actual dimension of the horn that has been used. After completing the model construction, it is then simulated in the CST transient time-domain solver to obtain the radiation pattern of the reflectarray. A broadside beam can only be formed if the reflectarray is working.

CHAPTER 3

DIELECTRIC RESONATOR REFLECTARRAY WITH BOTTOM-LOADING STRIP

3.1 Introduction

The use of dielectric resonator antenna (DRA) in reflectarray was first proposed in year 2000 (Keller, M. G. et al., 2000), where the length of a rectangular DRA was varied to bring about different phase shifts to the radiating elements. Since then, it is suggested the DRA reflectarray has many advantages such as low loss, broad bandwidth, low mutual coupling, good frequency response, and high radiation efficiency (Jamaluddin, M. H. et al., 2008; Jamaluddin, M. H. et al., 2009; Ahmadi, F. et al., 2013). The phase variation range of DRA radiating element is comparable with that for the microstrip radiating element.

Slot loading is one of the popular methods to generate phase shift in the DRA reflectarray element (Abd-Elhady, A. M. et al., 2010; Abd-Elhady, A. M. et al., 2012). In (Dzulkipli, N. I. et al., 2012), the bottom-loading slot was made into the shapes of alphabets. By varying different arm length of the complex-shaped slots, different reflection phases can be achieved in a single-dimensioned DRA element. Other simple slot-loading DRA reflectarray is also reported in (Zainud-Deen, S. H. et al., 2010). Slot was also combined with the

notched DRA for designing a dual-band reflectarray, operating in the C and X bands (Alsath, M. G. N. et al., 2012).

The DRA is also commonly used together with the microstrip elements such as patches and strips to form the phase-shifting radiating element (Jamaluddin, M. H. et al., 2008). In 2008, a patch-loaded DRA reflectarray was proposed in (Jamaluddin, M. H. et al., 2009), where a rectangular microstrip patch is stuck to the top surface of a DRA element. By varying the patch length while maintaining the patch width, the reflection phase of the top-loading DRA element can be varied. However, the fabrication process can be troublesome and the patch has to be manually attached to the top surface of the DRA.

Comparing with those published methods, a simpler way of phase-shifting mechanism has been proposed by loading a conductive strip beneath a DRA element. In this section, the design procedures mentioned in Chapter 2 will be employed for designing a DRA refectarray for a phase shift of 336^{o}, which is sufficient for many practical applications.

3.2 DRA Reflectarray with Underloading Strip

3.2.1 Unit Cell Configuration

In this chapter, a rectangular conductive strip with variable length is placed beneath a DR element for providing phase shift. It was found that strip with a different length is able to introduce a certain amount of additional phase to the reflected wave. The configuration of the DRA radiating element, with a dimension of 14mm (W) × 14mm (W) × 6mm (H), is shown in Figure 3.1. The DRA was made by a transparent glass with relative permittivity ε_r of 7 and loss tangent of 0.01. As can be seen from the figure, the metallic loading strips were first etched on the top surface of a FR4 substrate (with relative permittivity ε_r = 4.4, tanδ = 0.02, and thickness of h = 1.5 mm). The glass DRA is later stacked right on top of the strip by using glue and the strip can be designed into a number of lengths for achieving different phase shifts. To impose additional phase to the incident wave, the strip length S can provide a tuning freedom ranging from 2 mm until 13 mm. The gap beneath the DRA does not have significant effect on the performance, since it is in the range of micrometers. Comparing to the DRA reflectarray with a top-loading strip (Jamaluddin, M. H. et al., 2010), the manufacture of the proposed configuration is mechanically simpler. For those designs in (Jamaluddin, M. H. et al., 2010), the strip is to be manually fabricated on the top surface of the DRA. In my case, multiple strips can be directly etched on the FR4 substrate using the standard printed circuit board (PCB) technology. This makes the strip to have much precise dimension.

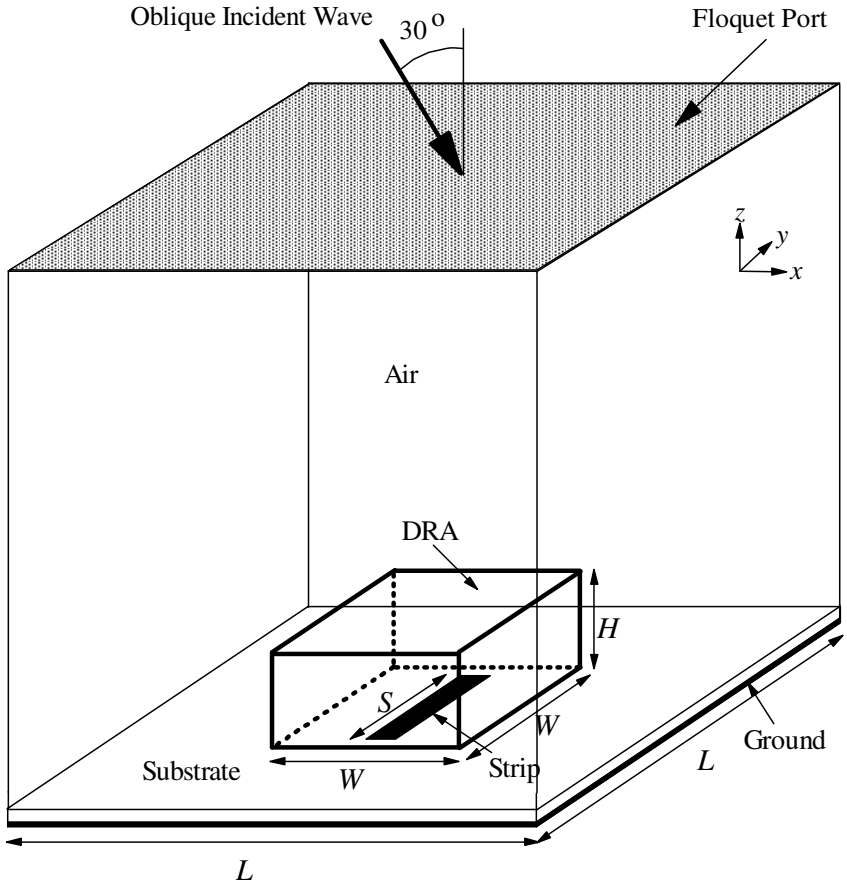

Figure 3.1: DRA radiating element with variable conductive strip

3.2.2 Unit Cell Simulation

The Floquet procedure (Abd-Elhady, A. M. et al., 2012) is now used for modeling the reflection characteristics of the unit cell, where the simulation was done by using Ansoft HFSS. In the simulation model, the incident wave is generated on the Floquet port at the top surface of the air-filled unit cell, as depicted in Figure 3.1. It has an inherent infinite periodic array approach (Abd-Elhady, A. M. et al., 2012) which can be used to expand the radiating element into an infinite periodic array in the *x*- and *y*-directions. In this case,

the coupling between the elements can get accounted for. This helps to produce a more accurate S Curve as the reflection phase is now calculated in the virtual array environment instead of considering only an isolated single element. The separation distance between any two DRAs is set to be 25.39mm (0.55 λ at 6.5 GHz) because it can maximize the range of the phase shift. Also, a square-shaped substrate is selected because the mirror images of DRA element will make all the elements (including the DRA and all its images) to have a distance of 0.55 λ in both the *x*- and *y*-directions, typical for optimizing the performance of an antenna array. This makes the design process much easier.

In simulation, the port is de-embedded near to the top surface of the DRA for a shorter traveling path so that the phase change can be kept below one cycle. Figure 3.2 shows the unit cell reflection magnitude and phase curves. It can be seen from the magnitude response that the reflection loss at the Floquet port maximizes when the length of the strip is 8.1 mm. This loss is caused by the resonance mode of the underloading strip, taking account into the overloading dielectric, which can observed from the fact that this mode stays even for DRA with different height. This signal loss is caused by the bottom-loading strip which resonates and absorbs part of the incident wave, which is unwanted but unavoidable. So, it is very crucial to minimize this loss. The strip length is the geometrical design parameter that changes the reflection phase. As it gets from 2 mm up to 13 mm (resolution of 0.1 mm), as can be seen, the reflection phase slides down from -45.7^{o} to -381.7^{o}, giving a variation range of 336^{o}, which is pretty much sufficient to compensate the

incident wave beams so that the reflected wave fronts can be aligned to form a plane wave. Oblique incidence angle of 30^{o} was considered in this unit cell simulation as the reflectarray is to be designed to have a side-fed horn with the same angle.

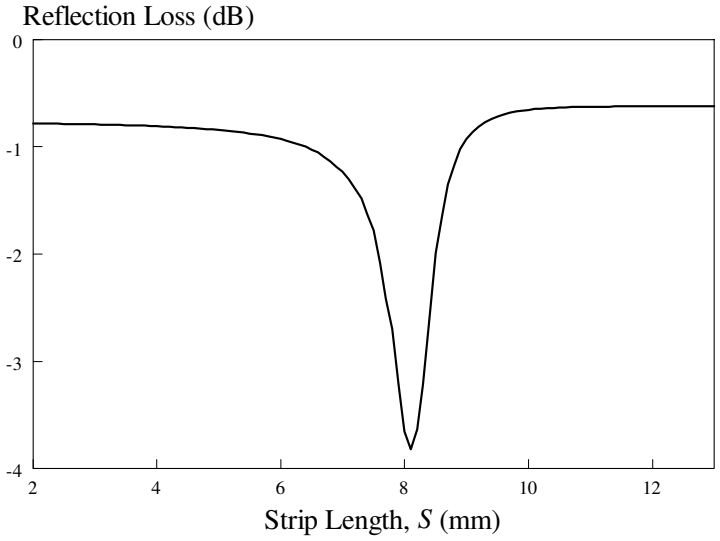

(a)

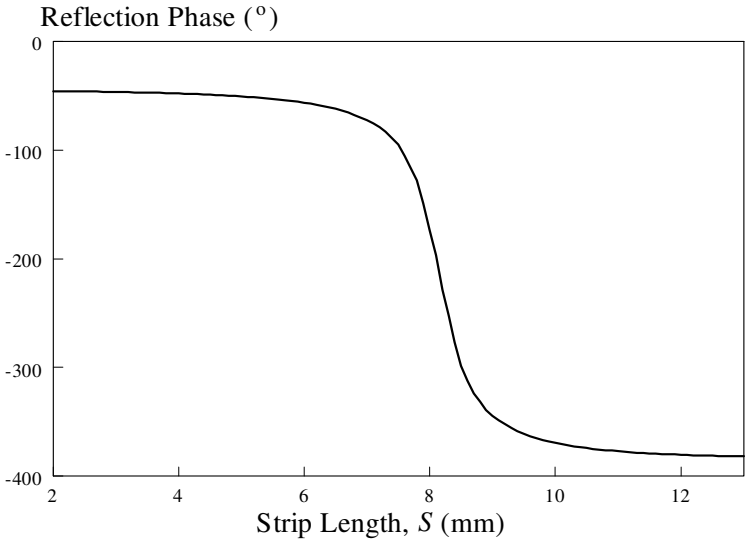

(b)

Figure 3.2: (a) Reflection loss and (b) reflection phase at 6.5 GHz as a function of strip length. (resolution = 0.1mm).

3.2.3 Design of Reflectarray

The next step is to design the DRA reflectarray. First, the reflection phases for all the unit elements are calculated for a certain feed horn setting. Then, the additional phase that is required by each of the elements is extracted. Finally, the "S Curve" in Figure 3.2 (b) is used to obtain the strip length that is required to give this additional phase.

3.2.3.1 Phase Calculation

A 7×7 DRA reflectarray will be designed, shown in Figure 3.3. The feed horn is aligned to $y = D / 2$ plane of the reflectarray, with the *E*-plane of the horn perpendicular to this *xz* - plane. Since the unit elements are placed at different path lengths from the feed horn, the incident wave will reach them at different time instants, making the reflected wave beams to have a multitude of phases. In this case, no plane wave can be formed. As the spacing of the unit cells is taken to be 0.55λ at 6.5 GHz, the proposed 7 × 7 reflectarray will have a dimension of D = 177.68mm, with each of the DRA placed d_1 = 25.38 mm (~ 0.55λ) apart from its neighboring counterparts. The feeding horn antenna was placed at f apart from the center of the grounded substrate and having an inclination angle of 30° to avoid blockage. The unit elements must be placed in the far-field zone of the feeder (Huang J. and Encinar, J. A., 2007). For this design, the *f/D* ratio of 1 is used to minimize the differences between the paths. The distance in this case is $f = D$ = 177.68 mm, being

greater than the minimum far-field (horn) requirement of 175.3 mm. Larger f causes the path length to increase.

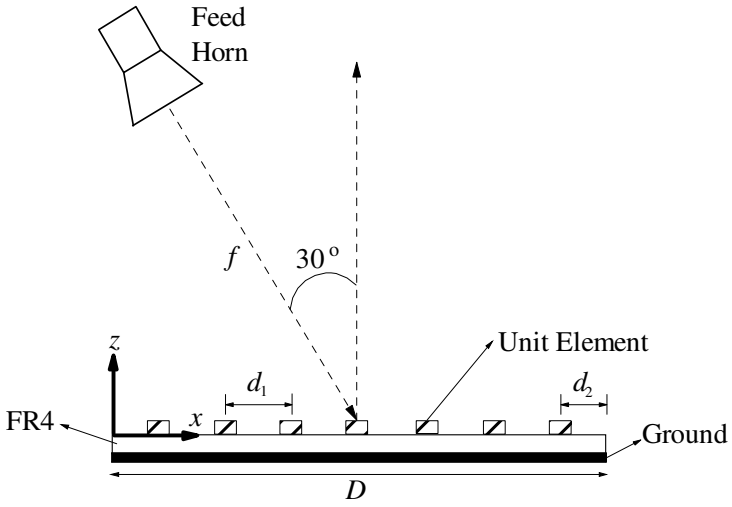

(a)

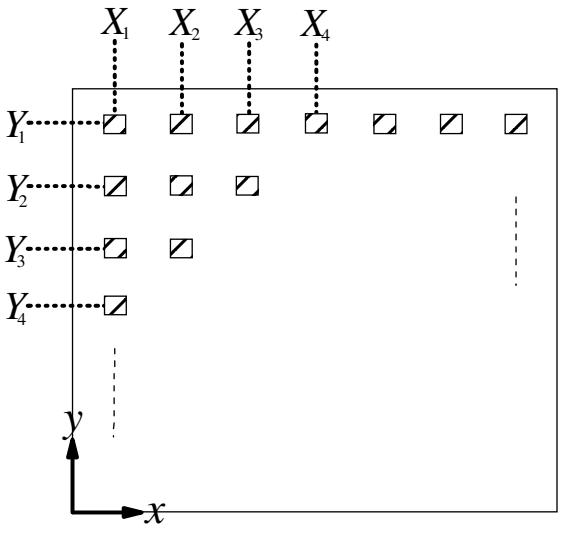

(b)

Figure 3.3: Configuration of the 7×7 DRA reflectarray with an undelaid strip as phase shifter. (a) Side view (b) Top view

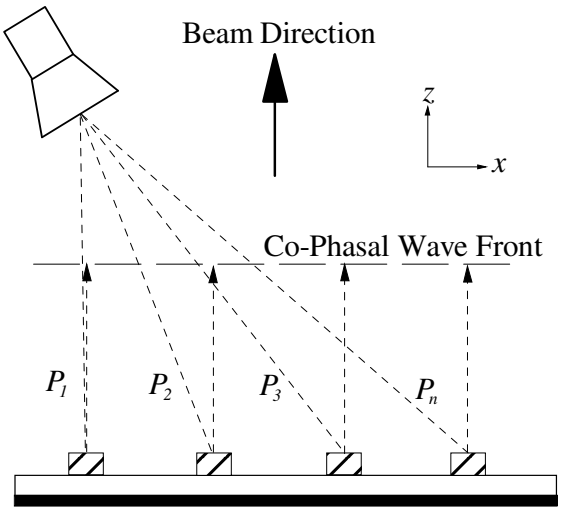

Figure 3.4: The path lengths formed by all the incident wave beams.

Referring to Figure 3.4, the travelling paths P_1, P_2, P_3,…, P_n are taken from the feed horn to the top surface of each of the DRA elements. By knowing the operating frequency at 6.5 GHz, the corresponding propagation phases for all the elements can be calculated. The path lengths and phases for all the forty nine elements are tabulated in Table 3.1.

Table 3.1: Path lengths and the corresponding propagation phases for all the unit elements of the DRA reflectarray

Path Length, (Propagation Phase)	x_1=12.69mm	x_2=38.07mm	x_3=63.45mm	x_4=88.83mm	x_5=114.21mm	x_6=139.59mm	x_7=164.97mm
y_1=12.69mm	172.15mm (1342.89°)	175.85mm (1371.78°)	183.03mm (1427.79°)	193.30mm (1507.92°)	206.20mm (1608.55°)	221.27mm (1726.12°)	238.10mm (1857.40°)
y_2=38.07mm	162.52mm (1267.81°)	166.44mm (1298.37°)	174.01mm (1357.41°)	184.78mm (1441.46°)	198.24mm (1546.42°)	213.87mm (1668.37°)	231.24mm (1803.86°)
y_3=63.45mm	156.46mm (1220.55°)	160.53mm (1252.26°)	168.36mm (1313.38°)	179.48mm (1400.06 °)	193.30mm (1507.92°)	209.30mm (1632.74°)	227.02mm (1770.96°)
y_4=88.83mm	154.39mm (1204.38°)	158.51mm (1236.50°)	166.44mm (1298.37°)	177.67mm (1385.99°)	191.63mm (1494.86°)	207.76mm (1620.69°)	225.60mm (1759.86°)
y_5=114.21mm	156.46mm (1220.55°)	160.53mm (1252.26°)	168.36mm (1313.38°)	179.48mm (1400.06 °)	193.30mm (1507.92°)	209.30mm (1632.74°)	227.02mm (1770.96°)
y_6=139.59mm	162.52mm (1267.81°)	166.44mm (1298.37°)	174.01mm (1357.41°)	184.78mm (1441.46°)	198.24mm (1546.42°)	213.87mm (1668.37°)	231.24mm (1803.86°)
y_7=164.97mm	172.15mm (1342.89°)	175.85mm (1371.78°)	183.03mm (1427.79°)	193.30mm (1507.92°)	206.20mm (1608.55°)	221.27mm (1726.12°)	238.10mm (1857.40°)

3.2.3.2 Extraction of Strip Lengths

In my design, the element which has the shortest path length (x_1 = 12.69 mm, y_4 = 88.83 mm) is taken to be the reference. The path length for the wave to travel from the horn to this element is 154.39mm which is equal to a propagation phase of 1204.4^o. Now, the element located at (x_7, y_7) has a propagation phase of 1857.4^o as the wave has travelled a farther distance of 238.1 mm. The phase difference between the two paths is 653.01^o (or equivalently 293.01^o). Since the element at (x_1, y_4) is taken to be the reference and it has under-loading strip length of 13 mm, the element at (x_7, y_7) will need a compensating phase of 293.01^o, which has an underloading strip of 7.4 mm as can be seen from the S Curve in Figure 3.2(b), to make it co-phasal with (x_1, y_4). By such token, other elements are compensated accordingly so that all will have the same phase as that at (x_1, y_4). The path differences described as phases and their corresponding strip lengths that are required by all elements are given in Table 3.2. With the under-loading strips to provide the additional phase shifts to all the elements, a co-phasal wave front can then be formed in the reflected wave, resulting a radiation beam pointing to the broadside direction ($\theta = 0^o$), as can be seen in Figure 3.4

.

Table 3.2: Additional phase shifts and compensating strip lengths that are required by all unit elements.

Phase Difference, (Strip length)	x_1=12.69mm	x_2=38.07mm	x_3=63.45mm	x_4=88.83mm	x_5=114.21mm	x_6=139.59mm	x_7=164.97mm
y_1=12.69mm	138.51° (8.26 mm)	167.39° (8.15 mm)	223.41° (7.95 mm)	303.53° (7.17 mm)	44.17° (8.88 mm)	161.73° (8.17 mm)	293.01° (7.40 mm)
y_2=38.07mm	63.43° (8.66 mm)	93.98° (8.45 mm)	153.03° (8.20 mm)	237.07° (7.87 mm)	342.04° (2.00 mm)	103.99° (8.40 mm)	239.47° (7.86 mm)
y_3=63.45mm	16.16° (9.72 mm)	47.87° (8.84 mm)	108.99° (8.37 mm)	195.68° (8.04 mm)	303.53° (7.17 mm)	68.36° (8.61 mm)	206.57° (8.00 mm)
y_4=88.83mm	0° (13.00 mm)	32.12° (9.11 mm)	93.98° (8.45 mm)	181.61° (8.11 mm)	290.48° (7.43 mm)	56.31° (8.72 mm)	195.47° (8.04 mm)
y_5=114.21mm	16.16° (9.72 mm)	47.87° (8.84 mm)	108.99° (8.37 mm)	195.68° (8.04 mm)	303.53° (7.17 mm)	68.36° (8.61 mm)	206.57° (8.00 mm)
y_6=139.59mm	63.43° (8.66 mm)	93.98° (8.45 mm)	153.03° (8.20 mm)	237.07° (7.87 mm)	342.04° (2.00 mm)	103.99° (8.40 mm)	239.47° (7.86 mm)
y_7=164.97mm	138.51° (8.26 mm)	167.39° (8.15 mm)	223.41° (7.95 mm)	303.53° (7.17 mm)	44.17° (8.88 mm)	161.73° (8.17 mm)	293.01° (7.40 mm)

3.2.3.3 Reflectarray Simulation Model

The strip lengths calculated in Table 3.2 will be used to construct the simulation model in Figure 3.5. The accuracy limit of this simulation is set to be -30dB. Further increase in the limit does not bring any obvious changes to the simulation result but significantly increases computation time. The commercial software CST Microwave Studio (CST Computer Simulation Technology AG, Microwave Studio) is used to verify the model because it's time domain solver has the capability to solve electrically large models. A high speed workstation Dell Precision T7500 (Intel (R) Xeon ® CPU with 24 GB RAM) is coupled with the NVIDIA Tesla C2070 (GPU computing supported) for performing all the simulations faster. To emulate the real case, a C-band pyramidal horn antenna (ATM PNR137-440-2, 5.85 GHz – 8.2 GHz) is included into the simulation model, as can be seen in Figure 3.5. It has a nominal antenna gain of 10dBi. However, simulation shows that the achievable antenna gain at 6.5 GHz is only 9.8 dBi with a half-power beamwidth (HPBW) of 73.2^{o}, and this value will be used in all the subsequent calculations. The horn has a dimension of 51.31mm (*H*) x 37.59mm (*E*) and the flare length F =73.5mm as shown in Figure 3.6. Also seen in the figure is the 7×7 reflectarray, with all the DRAs loaded with phase-shifting strips beneath. The photograph of the fabricated prototype is illustrated in Figure 3.7.

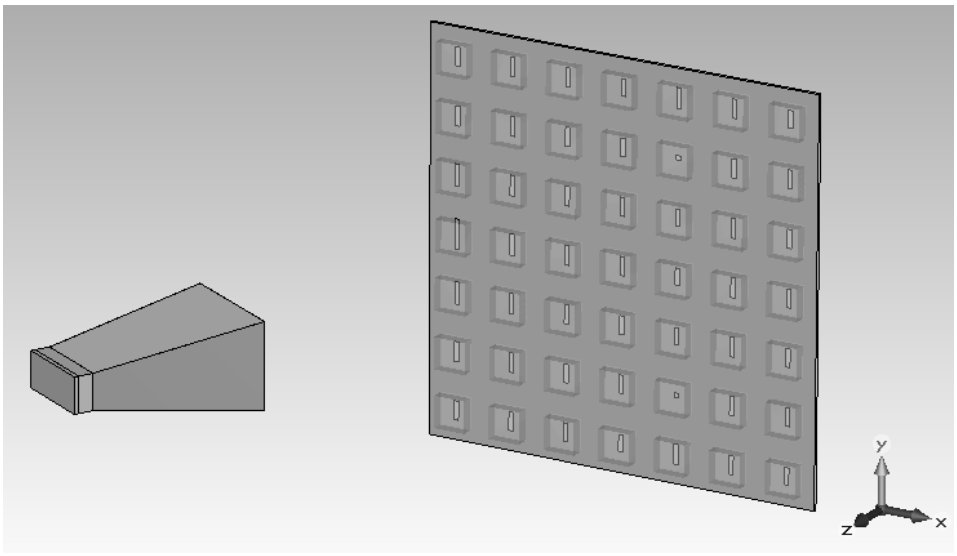

(a)

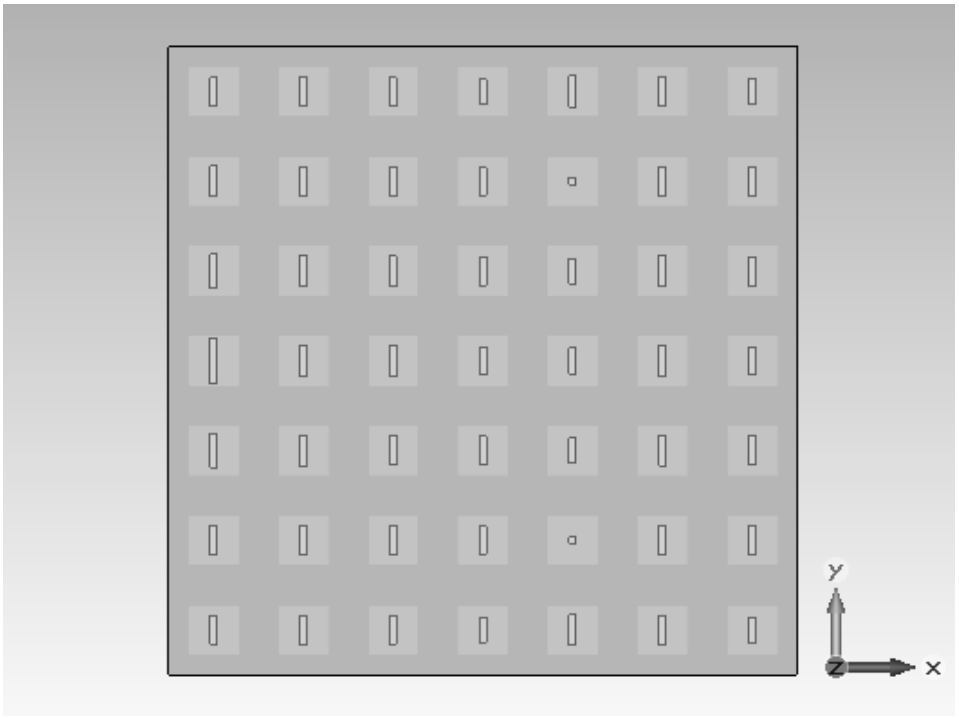

(b)

Figure 3.5: CST simulation model of the 7×7 DRA reflectarray. (a) Three-dimensional view. (b) Top view.

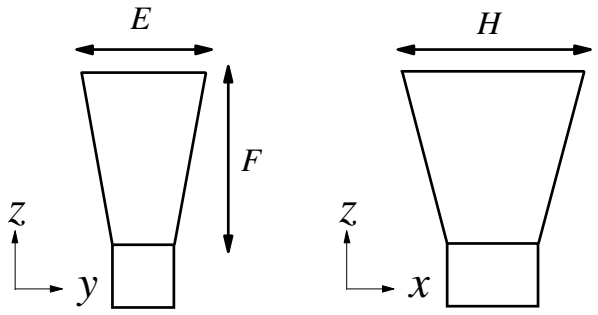

(a) (b)

Figure 3.6: Side views of the reflectarray's feeding horn antenna: (a) E-plane. (b) H plane

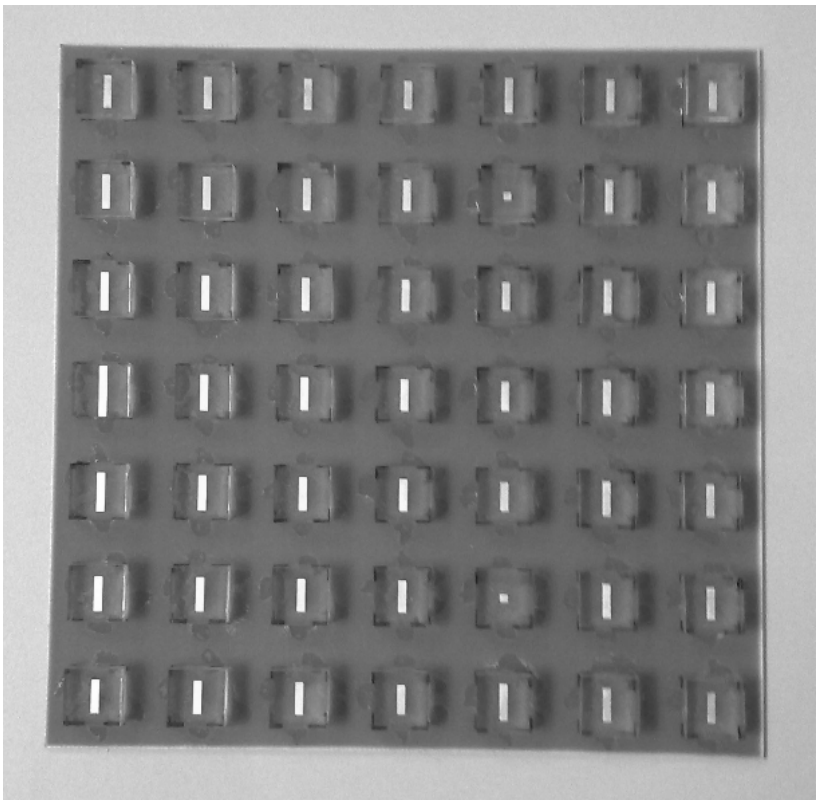

Figure 3.7: Photograph of the fabricated prototype. The strips are printed on the substrate and DRAs are stuck by using glue.

3.3 Reflectarray Measurement Method

The measurement setup for the reflectarray is illustrated in Figure 3.8. The Rohde & Schwarz SMB100A Signal Generator (100 kHz -12.75 GHz) is used to generate a monotone microwave signal and it is connected to the feed horn of the reflectarray. And the transmitted signal is received by a similar measuring horn antenna (ATM PNR137-440-2, 5.85 GHz – 8.2 GHz) which is rotated around the reflectarray at a fixed far-field distance of 3 m, with the received power read from an Advantest U3771 Spectrum Analyzer (9 kHz – 31.8 GHz). The reflectarray remains static throughout the measurement process. In all cases, the measuring horn antenna is always placed at a far-field distance (R = 3m) from the antenna under test.

The measurement procedure of the antenna gain is now described. With reference to Figure 3.8, the reflectarray is first replaced by a reference C-band horn and its transmitted power in the broadside direction ($\theta = 0^{o}$) is measured by a measuring horn. The transmitting horn is given with a constant input power of 10 dBm at 6.5 GHz and the received power is denoted as P_r^H. By replacing the reference horn with the reflectarray under test, the received power P_r^R at the measuring antenna is again recorded. Then, the received power of the reflectarray is compared to that of the reference horn. Since the gain of the reference horn (G_t^H) is already known (9.8 dBi); therefore the gain of the DRA reflectarray (G_t^R) can be obtained by the application of Friis Transmission Equation, as given in eqn. (3.1)

$$G_t^R = G_t^H + 10\log_{10}\left[P_r^R\right] - 10\log_{10}\left[P_r^H\right] \quad (3.1)$$

G_t^R : The antenna gain of the reflectarray under test.

G_t^H : The antenna gain of the reference horn.

P_r^R : The power received by the measuring horn from the reflectarray.

P_r^H : The power received by the measuring horn from the reference horn.

The radiation pattern can also be measured by using the same setting. Again, the measuring horn is positioned in the far-field region. By rotating the measuring horn at a fixed distance, now, the radiated power of the reflectarray is recorded for different elevation angles. Measurements around two major cut-planes are performed to obtain the antenna patterns.

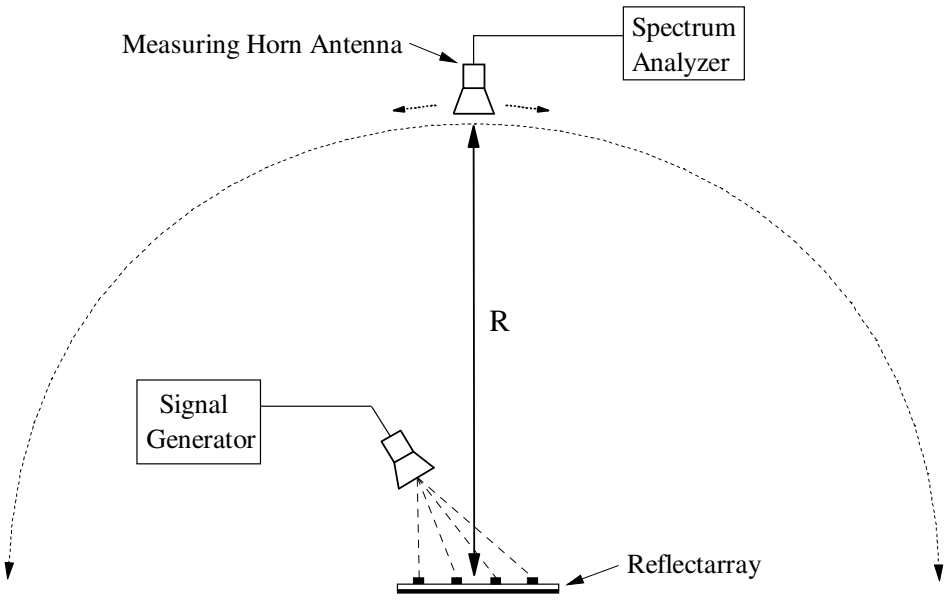

Figure 3.8: Measurement setup for the reflectarray. Signal generator was used to supply microwave signal to the reflectarray at 6.5 GHz, and spectrum analyzer was used for measuring the received power.

3.4 Results and Discussion

With the use of the measurement methods mentioned in Section 3.3, the simulated and measured radiation patterns of the proposed 7×7 DRA reflectarray are shown in Figure 3.9 with both the *xz* and *yz* planes. It has a maximum measured gain 14.35 dBi (simulation 16.2 dBi) in the broadside direction ($\theta = 0°$) at 6.5GHz. In the same direction, the co-polarized field is larger than its cross-polarized counterpart by ~ 30dB. Figure 3.10 shows the simulated and measured antenna gains across the frequency. The measured 1-dB gain bandwidth of the DRA reflectarray is 5.54% (simulation 6%).

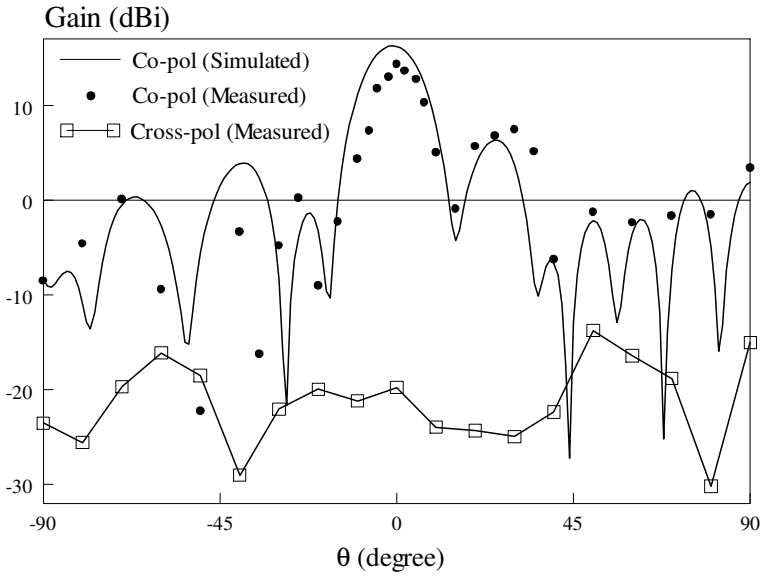

(a)

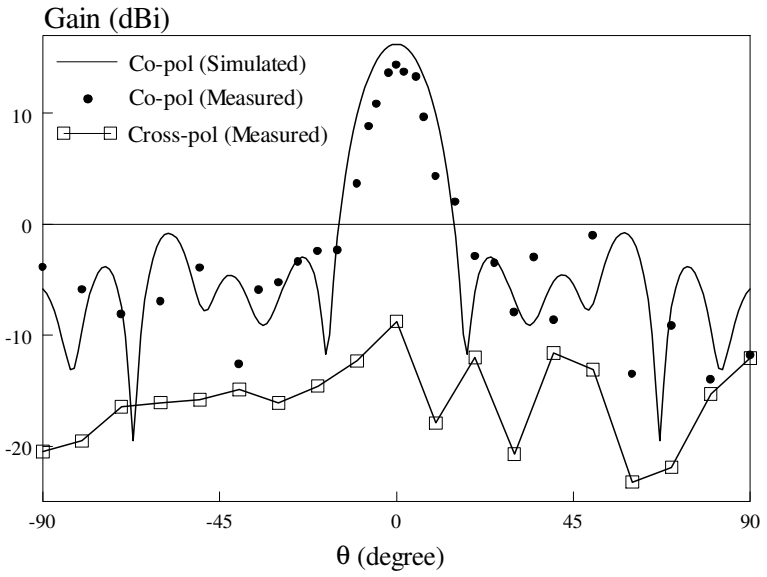

(b)

Figure 3.9: Simulated and measured (a) *xz*- and (b) *yz*- plane radiation patterns of the DRA reflectarray at 6.5GHz.

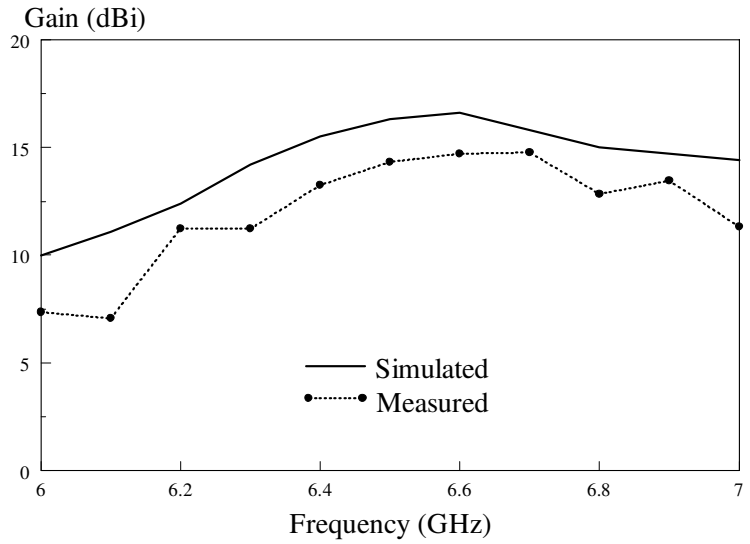

Figure 3.10: Simulated and measured 1-dB gain bandwidths of the DRA reflectarray.

3.5 Parametric Analysis

Parametric analysis of some of the crucial design parameters have been performed for both the unit cell and the reflectarray. This is because the reflection characteristics are only visible in the unit cell simulation. On the other hand, the radiation patterns can be analyzed by incorporating the feed horn.

3.5.1 DRA Unit Cell

3.5.1.1 Element Spacing

The effect of the from-center-to-center separation between any two DRA elements (d_1) can be visualized by varying the L dimension of the unit cells in the Floquet model for the configuration in Figure 3.1. The element spacing of the 7×7 DRA reflectarray was designed to be 0.55λ and now this distance is changed to study its effects. The reflection loss and S curves for separation distances of 0.50λ, 0.55λ, and 0.60λ are compared in Figure 3.11. The reflection losses maximize at around 8.1mm for all three separations. This is reasonable as this loss has been proven to be caused by the strip resonance. For the reflection phase, only minor changes are observed. The changeable phase range for designing a reflectarray slightly declines as the separation is varied. This also deteriorates antenna gain of the reflectarray.

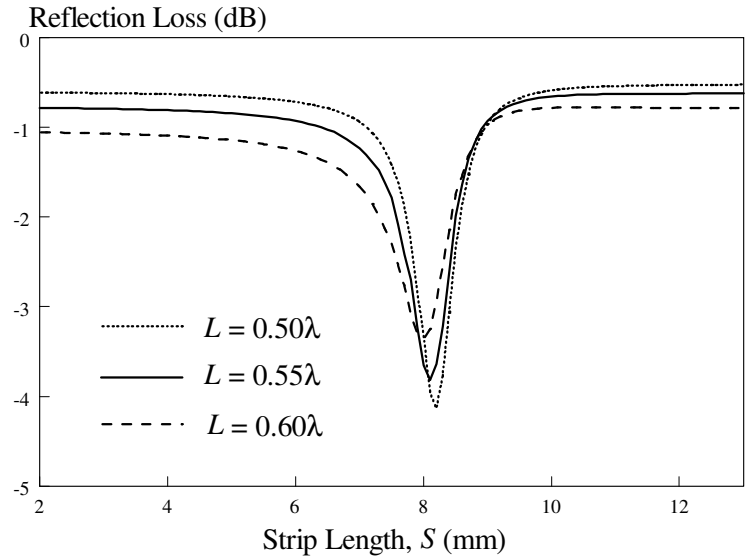

(a)

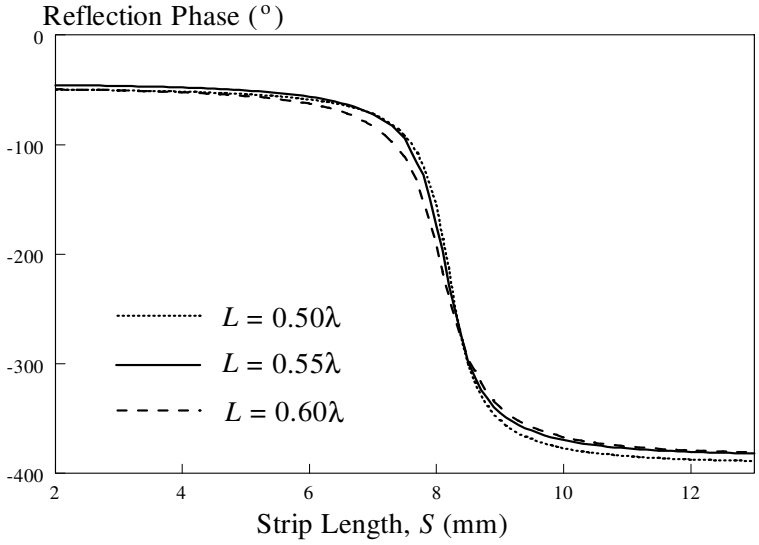

(b)

Figure 3.11: Reflection characteristics of the single DRA unit element for element spacing of 0.50λ, 0.55λ, and 0.60λ. (a) Reflection loss. (b) S Curve.

3.5.1.2 Operating Frequency

The DRA reflectarray and the single DRA element are both designed to operate at the center frequency of 6.5 GHz. By investigating the reflection characteristics of the unit element at different frequencies, we can estimate the performance of the reflectarray when the antenna is operating at frequencies other than 6.5 GHz. Figure 3.12 shows the reflection characteristics of the single DRA element at 6GHz, 6.5GHz and 7GHz. The reflection loss maximizes at 9 mm when the frequency of the incident wave is decreased to 6 GHz. On the other hand, it has the lowest loss at 7.7 mm for the incident frequency of 7 GHz. Again, this has confirmed that this loss is caused by the under-loading strip, causing part of the energy to disappear. With reference to Figure 3.12(b), the changeable range for the 6 GHz case increases slightly, with the price of much rapid changing rate around strip length of 9 mm in the S curve. This makes the design process difficult. On the other hand, for 7 GHz case, the S curve exhibits a slower gradient but the phase changeability becomes less, which is not desired. This shows the operating frequency of 6.5 GHz is the optimum since both the unit cell and reflectarray simulations are performed at 6.5 GHz.

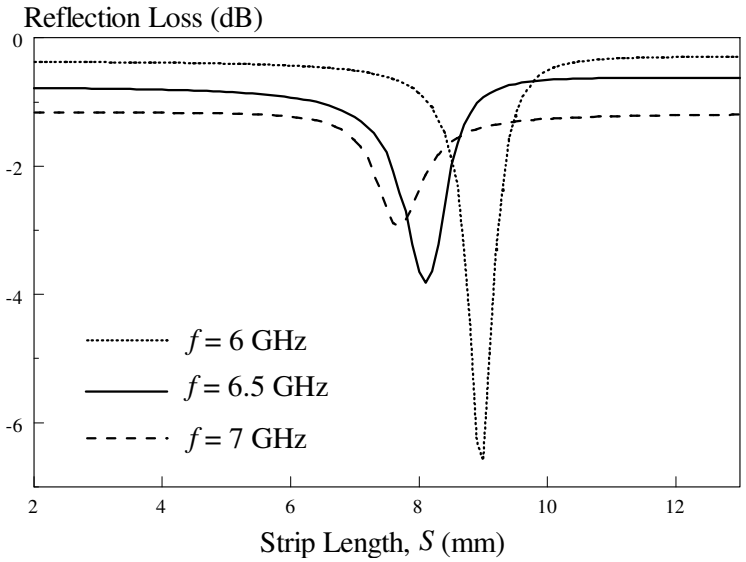

(a)

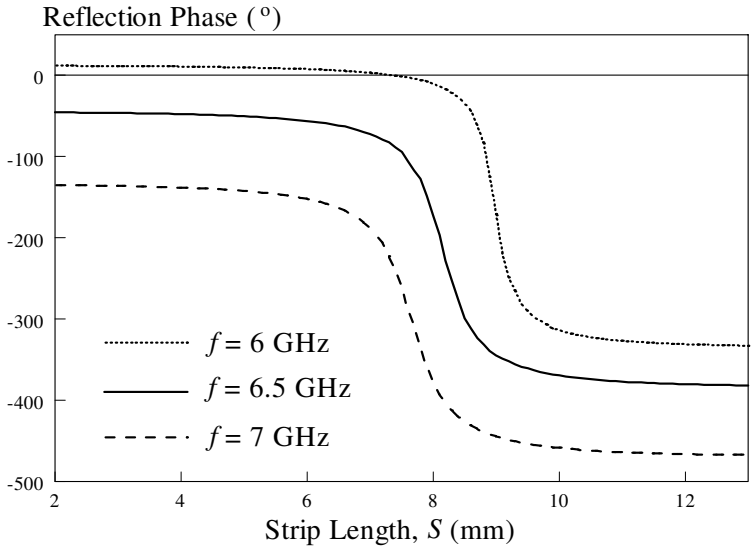

(b)

Figure 3.12: Reflection characteristics of the DRA unit element at 6 GHz, 6.5 GHz and 7 GHz. (a) Reflection loss. (b) S Curve.

3.5.2 DRA Reflectarray

3.5.2.1 *f/D* Ratio

By keeping all the design parameters for the case *f/D* = 1 unchanged, the *f/D* ratio of the proposed 7×7 DRA reflectarray is varied from 0.9 to 1.1. The radiation patterns (*xz* - plane) are generated for different *f/D* ratios as a function of the elevation angle and the results are shown in Figure 3.13. It can be seen from Figure 3.13 that the case for smaller *f/D* ratio has higher gain in the boresight direction as its feed horn is positioned nearer to the radiating elements, resulting weaker back lobe. However in this case, *f/D* =1 is selected as it can usually yield the best gain bandwidth (Huang J. and Encinar, J. A., 2007).

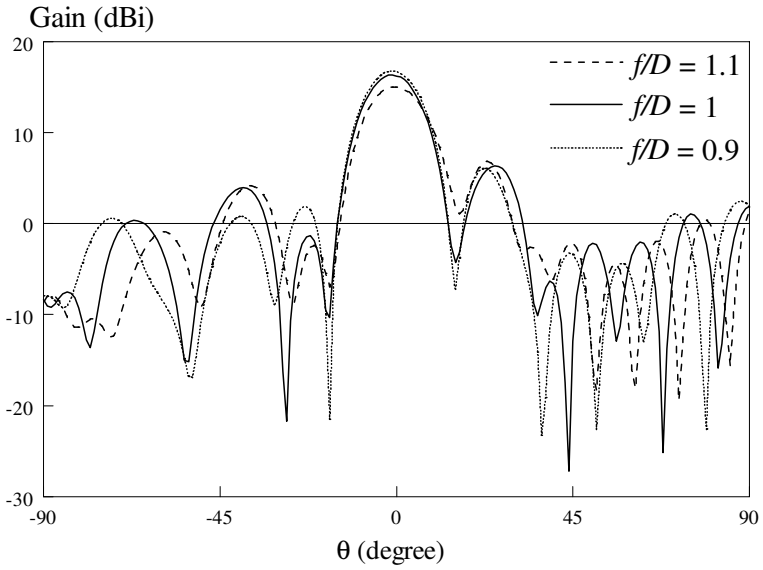

Figure 3.13: Radiation patterns of the DRA reflectarray with different *f/D* ratios at 6.5 GHz.

3.5.2.2 Operating Frequency

With the use of all the design parameters for the operating frequency of 6.5 GHz and the ratio of *f/D* = 1, radiation patterns have been generated for different feeding frequencies (*f* = 6.4 GHz, 6.5 GHz, and 6.6 GHz). It is to study the frequency tolerance of the reflectarray. It can be observed from Figure 3.14 that the antenna gain of the main lobe decreases when *f* goes lower. Although the cases for *f* = 6.5 GHz and 6.6GHz produces almost the same antenna gain, but side lobes of the reflectarray get higher with the increase.

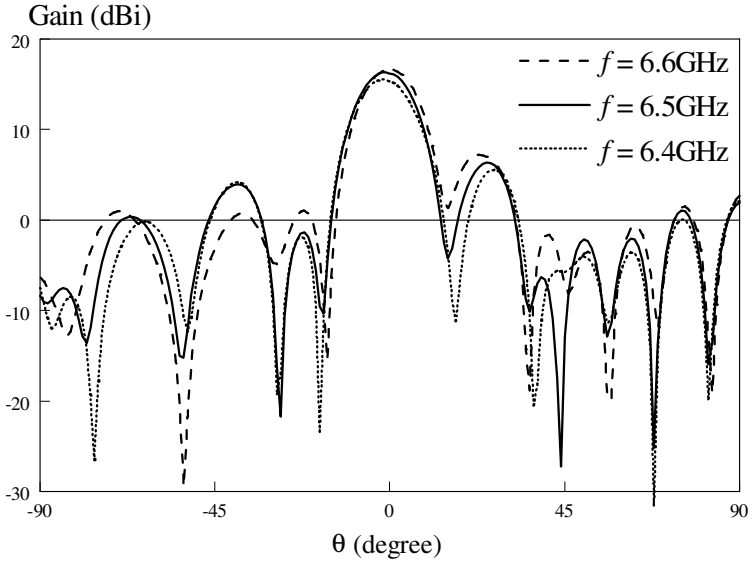

Figure 3.14: Radiation patterns of the DRA reflectarray at different frequencies.

3.6 Conclusion

DRA reflectarray loaded with a variable strip beneath the DRA has been proposed and its design procedure has been discussed. Simulation and experiment of the 7×7 DRA reflectarray have been carried out and good agreement between simulated and measured results is achieved. Based on the results, it is proven that the underlaid strip with variable length is able to function as a phase shifter for designing the DRA reflectarray.

CHAPTER 4

ELLIPTICAL AND CIRCULAR PATCH MICROSTRIP REFLECTARRAYS

4.1 Introduction

Microstrip patches are among the most popular choices for reflectarray due to some of the salient features such as flatness, compactness, and easy fabrication. The reflectarray proposed by Berry et al. (Berry, D. et al., 1963) did not receive much attention because it's cumbersome, being built by multiple metallic waveguide sections. This problem was alleviated with the introduction of microstrip reflectarray (Munson, R. E. et al., 1987), where the reflection phase of a square patch is varied by attaching a variable phase-delay line. Because of advantages such as light weight, compact, and easy to fabricate, it has inspired many other innovations since then.

A linearly polarized (LP) reflectarray usually requires an LP feeder. In 1992, Chang et al. (Chang D.-C. and Huang, M.-C., 1992) used the phase-delay line to design a high-gain LP microstrip patch reflectarray, but it has high cross polarization level. Later, this type of reflectarray was improved by arranging the bending direction of the phase delay lines symmetrically to reduce spurious radiation (Chang D.-C. and Huang, M.-C., 1995). Recently, in (Arrebola, M. et al., 2008), multiple LP feeders were used to excite a printed

microstrip reflectarray for generating multiple beams, each of them is able to work in any LP operation.

The first CP reflectarray was proposed by J. Huang and R. J. Pogorzelski in 1997 (Huang J. and Pogorzelski, R. J., 1997). In this ground-breaking work, the identical square patches attached with delay lines with a fixed length are rotated at different angles to generate phase shifts for circular polarization (CP) (Huang J. and Pogorzelski, R. J., 1998). Similar idea was demonstrated in the circular patch in (Adel, S. and Hammad, H., 2013). The CP reflectarray with rotated ring elements was proposed in (Han C. and Chang, K., 2003). In this design, two gaps are introduced on a circular ring to divide it into two. And the rotation of this ring was shown generating right-handed CP.

The main limitation of the microstrip reflectarray is narrow bandwidth. This is caused by the inherent narrow bandwidth nature of its microstrip element. Recently, broadening the bandwidth of reflectarray has become a popular research trend in this field. To improve the bandwidth of reflectarray, (Pozar, D. M., 2003) and (Encinar J. A. and Zornoza, J. A., 2003) have come up with the idea of using the multilayer stacked radiating elements. Here, several layers of substrates printed with microstrip elements are stacked together. It was claimed in (Zhao, M.-Y. et al., 2013) that the CP bandwidth of a reflectarray can be increased by combining two radiating elements with different sizes into one. This chapter has proposed the use of the elliptical patches to design an LP reflectarray. It comes along with a circular patch reflectarray for comparison. A foam-backed substrate is used to obtain a

broader bandwidth. The performances of the patch reflectarrays are compared in this chapter.

4.2 Elliptical Patch Reflectarray with Double-layered Substrate

4.2.1 Unit Cell Configuration

An elliptical microstrip patch, with major axis of A and minor axis of B, will now be used as the unit element for designing a linearly polarized reflectarray to work at 6.5 GHz, with the proposed configuration shown in Figure 4.1. The proposed unit patch is built on the top surface of a square FR4 substrate (L = 27.69 mm = 0.6λ at 6.5 GHz) with relative permittivity of ε_{rs} = 4.4 and thickness of h_1 = 1.5 mm. The metallic layer is etched away at the bottom surface of the substrate. With reference to the figure, one piece of foam with relative permittivity of ~ 1 and thickness of h_2 = 2 mm is inserted in between the substrate and a ground plane to imitate the air layer beneath the substrate, which is introduced for slowing down the changing rate of the reflection phase (will be shown later). In this case, the major axis (A) is varied from 0.6 mm to 27.4 mm while the minor axis (B) is fixed at 12mm. The maximum bound that A can reach is 0.6λ, which is also the size of the unit cell. The elliptical patch is placed such that its major axis is parallel to the E plane of the feed horn. By doing so, varying the major axis enables the introduction of additional phase shift to the incident wave beam.

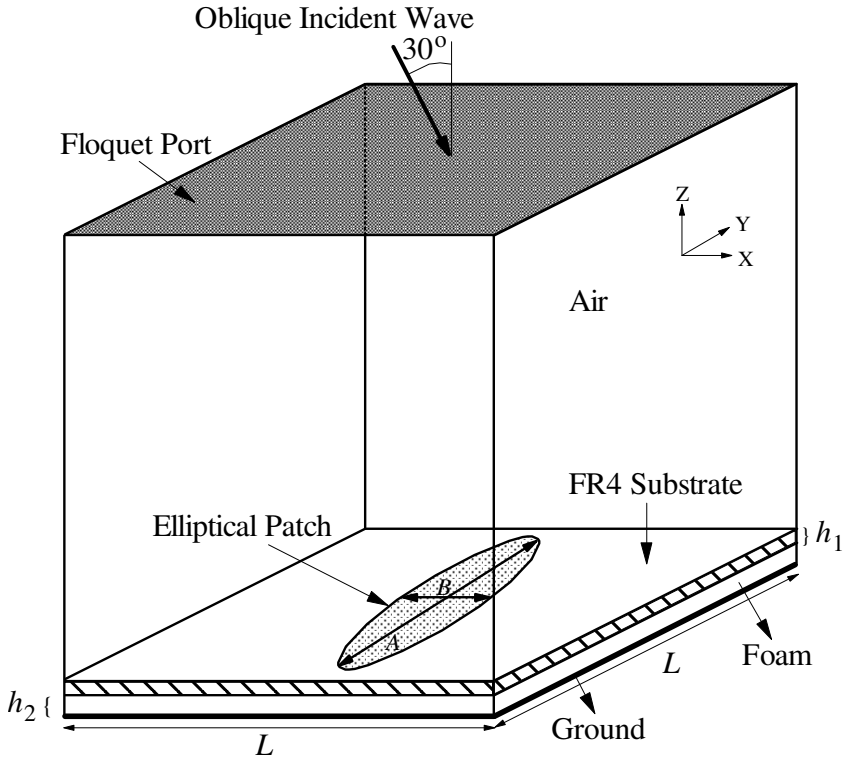

Figure 4.1: Unit cell for the elliptical patch with a double-layered substrate.

4.2.2 Unit Cell Simulation

Ansoft HFSS was used to simulate the reflection characteristics of the elliptical patch unit cell. Again, the single aforementioned unit cell is modeled by using the Floquet procedure mentioned in Section 3.2.2, with the corresponding setup shown in Figure 4.1. The reflection characteristics of the reflectarray can be visualized in this simulation. Figure 4.2 shows the reflection loss and S Curve of the elliptical patch element. Again, the dip (maximum loss of -1.26 dB) at A = 14.4 mm shown in Figure 4.2(a) corresponds to the resonance of the patch at 6.5 GHz, which is quite low to be ignored. Figure 4.3(b) is the reflection phase of the elliptical patch element. Changeable phase range of 318.2° is achievable with varying the length A,

which is less than the full phase range of 360° but is sufficient for my design. In the later part of this chapter, it will be shown that a phase range of 318.2° is already sufficient for designing a reflectarray with acceptable gain performance and accurate beam scanning angle.

By removing the air layer (or h_2 = 0 mm), the reflection characteristics of the elliptical patch element is studied. For this case, the cell length is reduced to $L = 0.3\lambda$ as that for 0.6λ is not able to provide sufficient phase shift (only ~ 17^o) when changing the major axis. Therefore, the center-to-center element spacing of this single-layered configuration is set to be 0.3λ (equal to L) at 6.5 GHz to achieve a phase range of 327.5^o. Figure 4.3 shows the reflection characteristics of the single-layered elliptical patch element along with the double-layered one. The phase curve for the single-layered case shows a much steeper phase change than the double-layered one, which is undesirable. Slow change is good as the reflectarray is now less affected by the fabrication tolerances since the sizes of the phase-changing elements are more distinguishable.

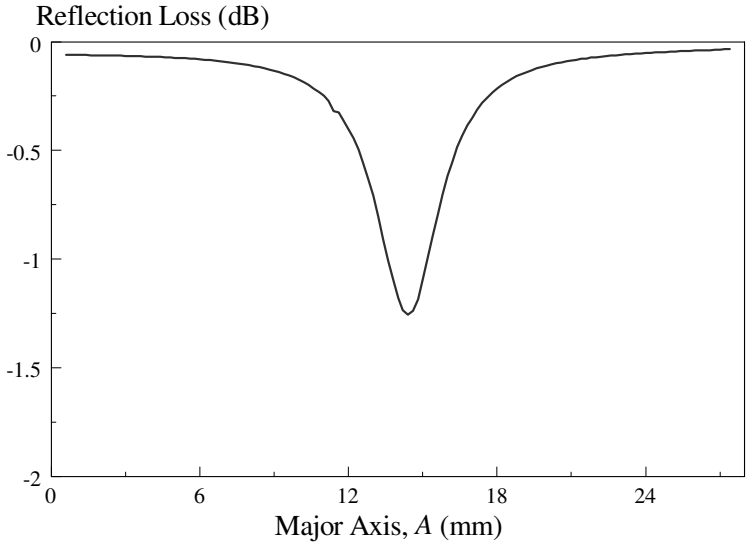

(a)

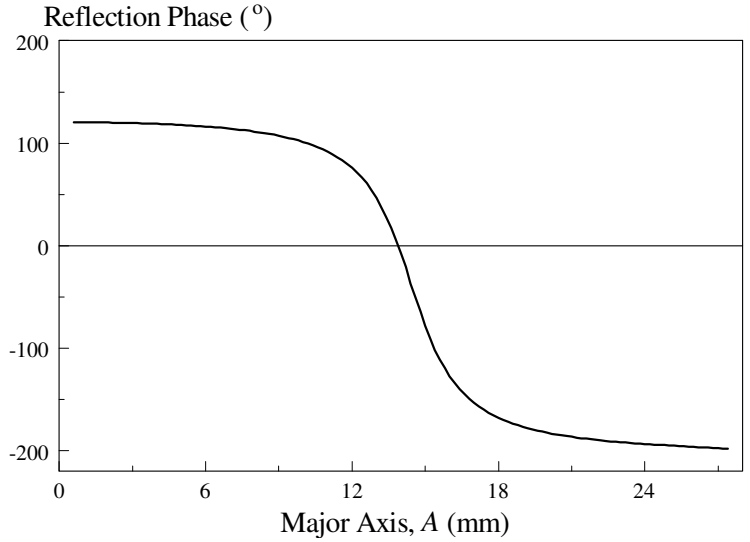

(b)

Figure 4.2: (a) Reflection loss and (b) reflection phase of the double-layered elliptical patch as a function of the major axis A at 6.5 GHz. (resolution = 0.2 mm).

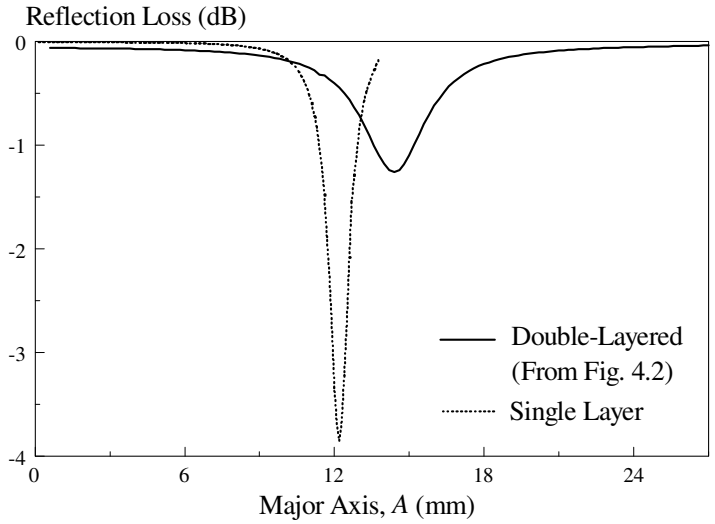

(a)

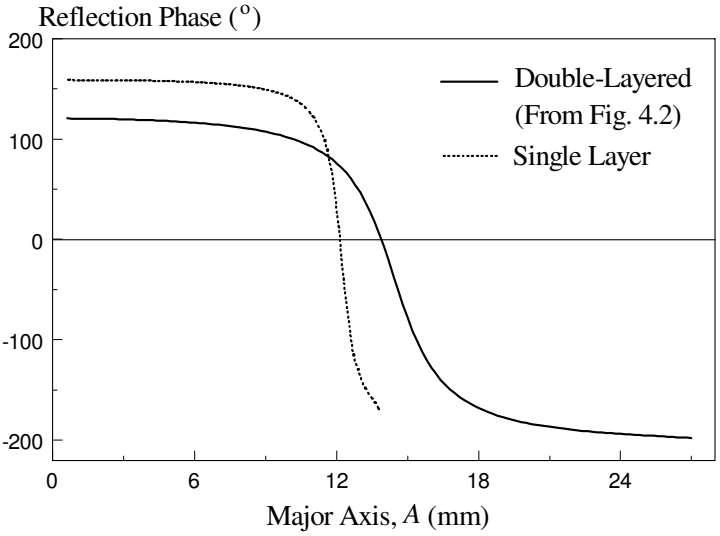

(b)

Figure 4.3: (a) Reflection loss and (b) reflection phase of the single-layered elliptical patch as a function of the major axis A at 6.5 GHz. (resolution = 0.2 mm). For ease of comparison, those for the double-layered case are also given.

4.3 Circular Patch Reflectarray with Double-layered Substrate

4.3.1 Unit Cell Configuration

With identical configuration, the elliptical patch is now replaced by the circular one, working as a linear antenna at the center frequency of 6.5 GHz. The same FR4 substrate (ε_{rs} = 4.4, h_1 = 1.5mm, and L = 27.69 mm = 0.6λ at 6.5 GHz) is used for the design, with the proposed structure shown in Fig. 4.4. Likewise, the metal layer at the bottom surface of the substrate is etched away, underpinning with air gap of h_1 = 2 mm. Now, the patch radius (R) is made a variable changeable from 0.1 mm to 13.8 mm to provide a phase-shifting range of 319.6^o to the incident wave.

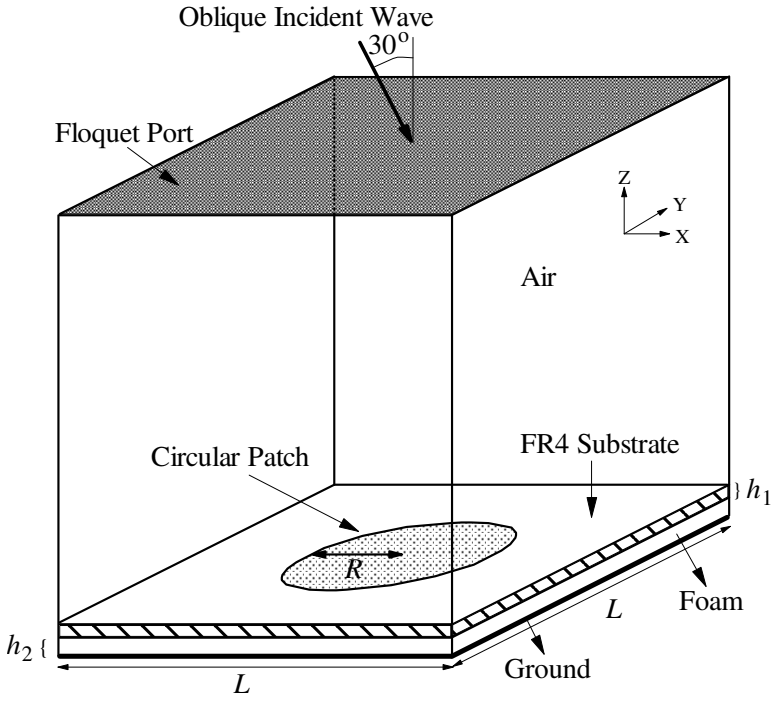

Figure 4.4: Unit cell for the circular patch with a double-layered substrate.

4.3.2 Unit Cell Simulation

Again, the commercial software Ansoft HFSS is used for analyzing the reflection characteristics of the unit cell. When translated into array with the use of Floquet Method, this setting is equivalent to an infinite reflectarray with a center-to-center element spacing of 0.6λ. With reference to Figure 4.5(a), the reflection loss peaks at -1.15dB at R = 7.2mm. Again, the patch resonates around 6.5 GHz at this dimension, causing extra loss to the incident wave. Figure 4.5(b) is the simulated S-Curve with varying R. Observed is that more phase shift can be induced around the resonance dimension of the patch, giving a total range of 319.6^{o}.

With the removal of the air gap, or by letting h_2 = 0 mm, the reflection characteristics is simulated for ease of comparison. For this case again, a shorter cell length is adopted L = 0.3λ so that a sufficient phase-shifting range is producible. This implies a closer patch separation when translated into virtual infinite array. Now, the reflection loss is generated by changing the radius of the single-layered patch unit and the result is shown in Figure 4.6(a). A lower magnitude of reflection coefficient at about -2.9dB is observed if compared to the double-layered case. The S-Curve simulation in Figure 4.6(b) shows that the phase shift of the single layer element goes much more rapid at around the resonance although it has a slightly broader range of 321.3^{o}. The stopper length at 6.9mm (~0.3 λ) corresponds to the maximum radius the circular patch can reach, for the element spacing of 0.3 λ.

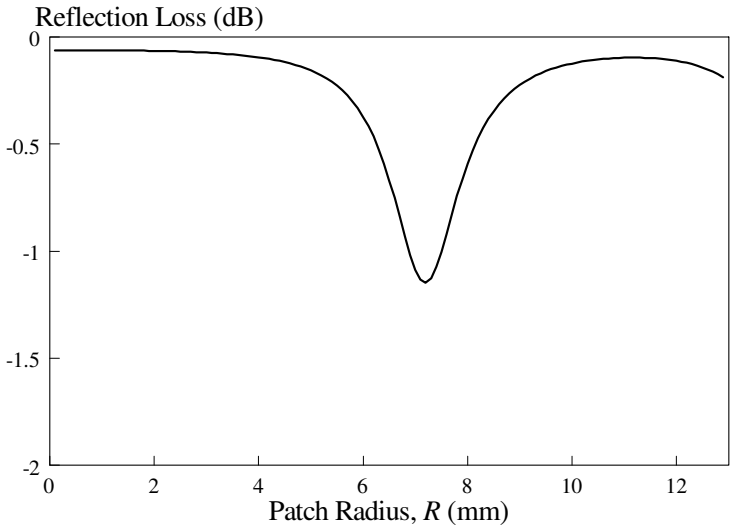

(a)

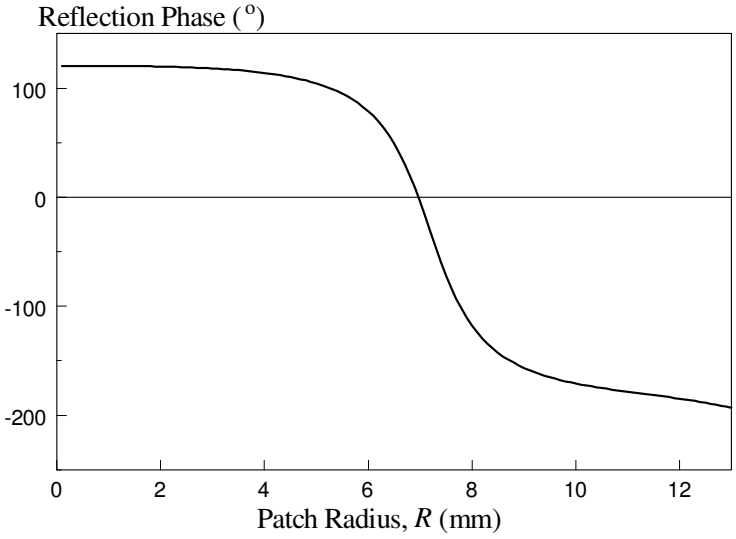

(b)

Figure 4.5: (a) Reflection loss and (b) reflection phase of the double-layered circular patch as a function of the major axis *A* at 6.5 GHz. (resolution = 0.1 mm).

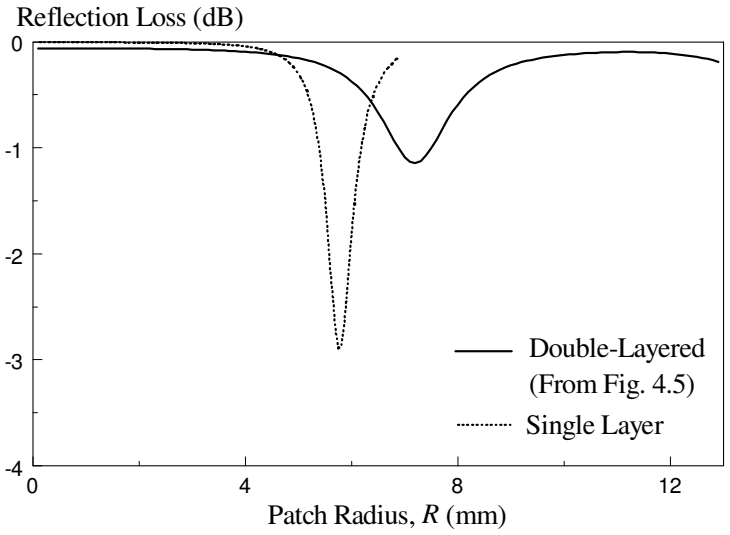

(a)

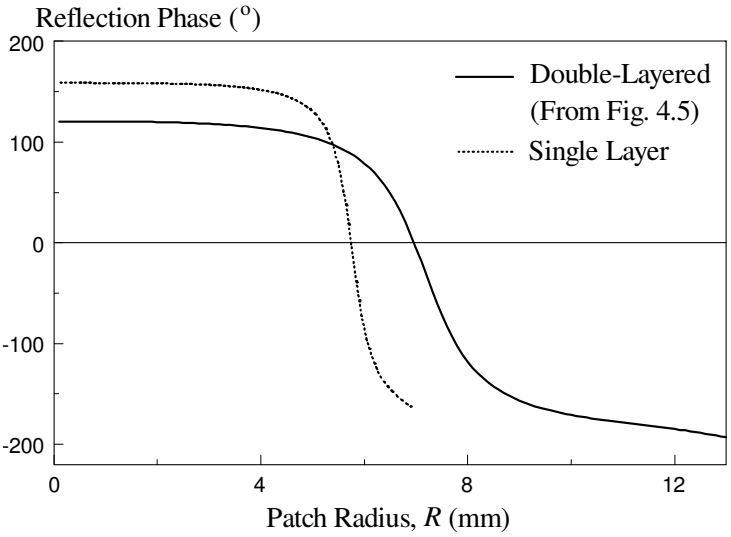

(b)

Figure 4.6: (a) Reflection loss and (b) reflection phase of the single-layered circular patch as a function of radius R at 6.5 GHz. (resolution = 0.1 mm). For ease of comparison, those for the double-layered case are also given.

4.4 Design of Reflectarray

With the information available in Section 4.2 and 4.3, the phase shifts that are required by the unit elements can now be calculated. Here, the dimensions of the circular and elliptical patches will be determined separately from their respective S-Curves.

4.4.1 Phase Calculation

For both cases, the aforementioned patches are used to design the 9 × 9 reflectarrays. The configuration of the proposed structure is shown in Figure 4.7. The incident wave will reach the unit elements at different time instants as they have different path length with respect to the feed horn, which is suspended with an inclination angle of 30^{o} with respect to the reflectarray. No plane wave can be formed in the broadside direction ($\theta = 0^{o}$). In this case, the spacing in between any two elements is taken 0.6λ at 6.5 GHz, resulting a reflectarray dimension of D = 249.21 mm. Again, it is fed by a linearly polarized C-band pyramidal horn suspended at a distance of f = 193.83 mm (minimum far-field distance of the horn is 175.3 mm) from the center point of the reflectarray with an inclination angle of 30^{o}. The feed horn is aligned to $y = D / 2$ plane of the reflectarray, with the E-plane of the horn orthogonal to this xz - plane. The offset feed configuration avoids the blockage of main radiation beam of the reflectarray in the broadside direction. Feed blockage usually introduces significant degradation in performance. Here, the f / D ratio is set to be 0.78 for a higher antenna gain.

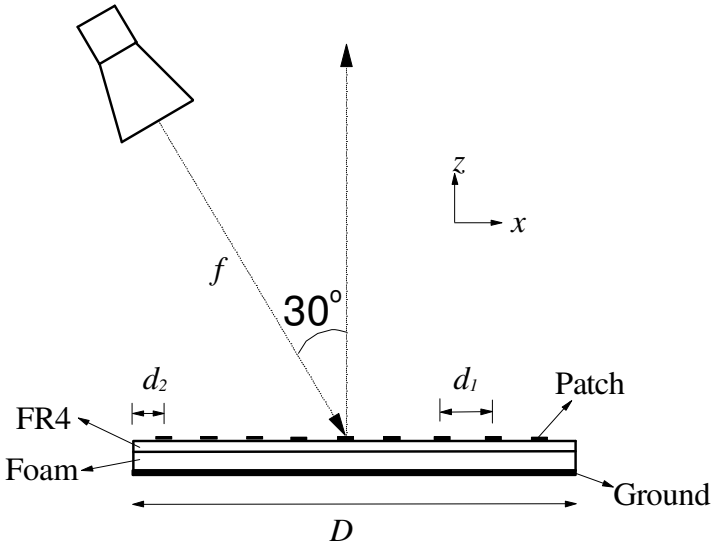

(a)

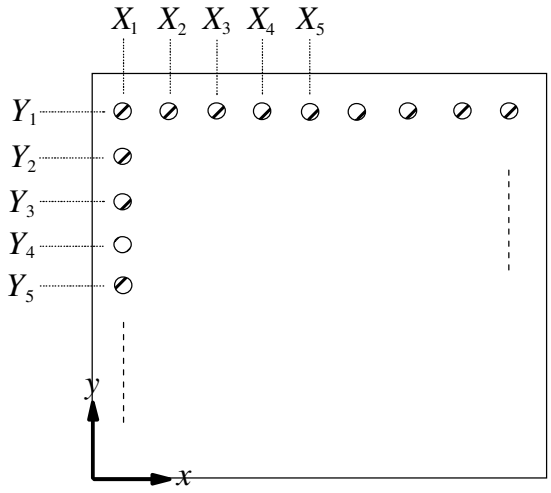

(b)

Figure 4.7: Configuration of the 9 × 9 patch reflectarray. (a) Side view. (b) Top view.

Taking the position (X_5, Y_5) to be the reference, the travelling paths from the horn to the patch elements are defined to be P_1, P_2,…P_n, as can be seen from Figure 4.8. With the center operating frequency of 6.5 GHz, the path lengths and their corresponding propagation phases are tabulated in Table 4.1. Comparing with the DRA reflectarray in Chapter 3, the difference of the propagation phase maximizes at 2255^o at the corner as the path length becomes longer when the antenna size is increased.

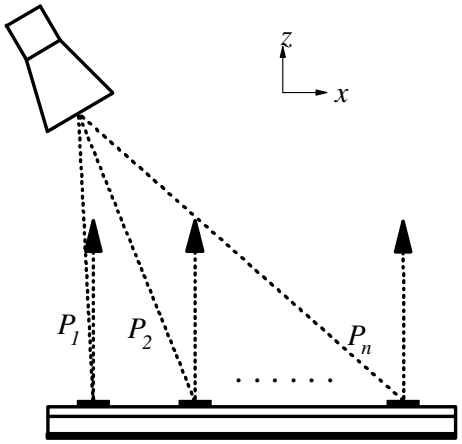

Figure 4.8: The path lengths formed by all the incident wave beams.

Table 4.1: Path lengths and the corresponding propagation phases for all the unit elements of the patch reflectarray

Position, (Propagation phase)	X_1=13.8 mm	X_2=41.5 mm	X_3=69.2 mm	X_4=96.9 mm	X_5= 124.6 mm	X_6=152.3 mm	X_7=180.0 mm	X_8=207.7 mm	X_9=235.3 mm
Y_1=13.8 mm	201.5 mm (1572.4°)	201.5 mm (1572.4°)	205.3 mm (1601.8°)	212.6 mm (1659.1°)	223.2 mm (1741.4°)	236.5 mm (1845.4°)	252.2 mm (1967.8°)	269.8 mm (2105.2°)	289.0 mm (2255.0°)
Y_2=41.5 mm	187.8 mm (1464.9°)	187.8 mm (1464.9°)	191.8 mm (1496.4°)	199.6 mm (1557.5°)	210.8 mm (1644.9°)	224.9 mm (1754.7°)	241.3 mm (1883.0°)	259.7 mm (2026.2°)	279.6 mm (2181.4°)
Y_3=69.2 mm	177.3 mm (1383.0°)	177.3 mm (1383.0°)	181.5 mm (1416.3°)	189.8 mm (1480.8°)	201.5 mm (1572.4°)	216.2 mm (1687.0°)	233.3 mm (1820.0°)	252.2 mm (1967.8°)	272.7 mm (2127.3°)
Y_4=96.9 mm	170.6 mm (1331.5°)	170.6 mm (1331.5°)	175.1 mm (1366.0°)	183.6 mm (1432.7°)	195.7 mm (1527.3°)	210.8 mm (1644.9°)	228.3 mm (1781.1°)	247.6 mm (1931.9°)	268.4 mm (2094.1°)
Y_5=124.6 mm	168.4 mm (1313.8°)	168.4 mm (1313.8°)	172.9 mm (1348.9°)	181.5 mm (1416.3°)	193.8 mm (1511.9°)	209.0 mm (1630.7°)	226.6 mm (1768.0°)	246.1 mm (1919.8°)	267.0 mm (2083.0°)
Y_6=152.3 mm	170.6 mm (1331.5°)	170.6 mm (1331.5°)	175.1 mm (1366.0°)	183.6 mm (1432.7°)	195.7 mm (1527.3°)	210.8 mm (1644.9°)	228.3 mm (1781.1°)	247.6 mm (1931.9°)	268.4 mm (2094.1°)
Y_7=180.0 mm	177.3 mm (1383.0°)	177.3 mm (1383.0°)	181.5 mm (1416.3°)	189.8 mm (1480.8°)	201.5 mm (1572.4°)	216.2 mm (1687.0°)	233.3 mm (1820.0°)	252.2 mm (1967.8°)	272.7 mm (2127.3°)
Y_8=207.7 mm	187.8 mm (1464.9°)	187.8 mm (1464.9°)	191.8 mm (1496.4°)	199.6 mm (1557.5°)	210.8 mm (1644.9°)	224.9 mm (1754.7°)	241.3 mm (1883.0°)	259.7 mm (2026.2°)	279.6 mm (2181.4°)
Y_9=235.3 mm	201.5 mm (1572.4°)	201.5 mm (1572.4°)	205.3 mm (1601.8°)	212.6 mm (1659.1°)	223.2 mm (1741.4°)	236.5 mm (1845.4°)	252.2 mm (1967.8°)	269.8 mm (2105.2°)	289.0 mm (2255.0°)

4.4.2 Dimension Extraction and Reflectarray Model

4.4.2.1 Elliptical Patch Reflectarray

Referring to Table 4.1, the propagation phase for the wave to reach the reference position (x_1, y_5) is 1313.8°. The element at the corner (x_9, y_9) has a longer path length with a propagation phase of 2255°. The phase difference between the two points is 941.2° (or equivalent to 221.2°). It can be seen from the S-Curve in Figure 4.2(b) that the reference elliptical patch has a major axis of A = 27 mm; as a result, the patch at (x_9, y_9) will have to be designed to have A = 13.48 mm in order to be able to provide a compensating phase of 221.2°. In Table 4.2, the phase differences for all elements comparing with the reference are calculated. Also furnished in the table is the major axis' of the patches that are required to compensate the required phases. Figure 4.9 is the simulation model of the 9 × 9 elliptical reflectarray with its feed horn. The photograph of the prototype is illustrated in Figure 4.10.

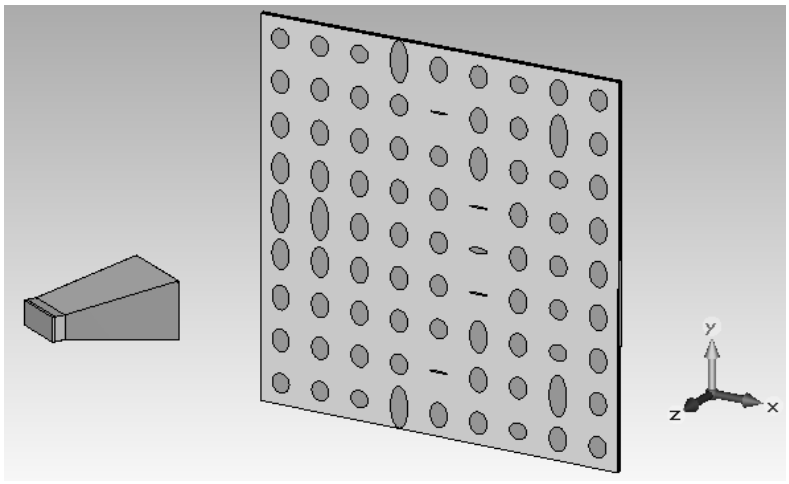

Figure 4.9: Simulation model of elliptical patch reflectarray

Table 4.2: Additional phase shifts and the elliptical patch dimensions that are required to compensate the incident wave beams.

Phase difference, (Major Axis)	X_1=13.8mm	X_2=41.5mm	X_3=69.2mm	X_4=96.9mm	X_5= 124.6mm	X_6=152.3mm	X_7=180.0mm	X_8=207.7mm	X_9=235.3mm
Y_1=13.8mm	258.6° (12.6 mm)	258.6° (12.6 mm)	288° (11.12 mm)	345.2° (27 mm)	67.5° (16.08 mm)	171.6° (14.26 mm)	293.9° (10.58 mm)	71.4° (15.96 mm)	221.2° (13.48 mm)
Y_2=41.5mm	151.1° (14.54 mm)	151.1° (14.54 mm)	182.6° (14.11 mm)	243.7° (13.02 mm)	331.1° (1 mm)	80.9° (15.73 mm)	209.1° (13.7 mm)	352.3° (27 mm)	147.6° (14.59 mm)
Y_3=69.2mm	69.1° (16.03 mm)	69.1° (16.03 mm)	102.5° (15.28 mm)	166.9° (14.32 mm)	258.6° (12.6 mm)	13.1° (20.46 mm)	146.1° (14.61 mm)	293.9° (10.58 mm)	93.4° (15.45 mm)
Y_4=96.9mm	17.6° (19.53 mm)	17.6° (19.53 mm)	52.2° (16.6 mm)	118.9° (15 mm)	213.4° (13.62 mm)	331.1° (1 mm)	107.3° (15.19 mm)	258° (12.62 mm)	60.3° (16.32 mm)
Y_5=124.6mm	0° (27 mm)	0° (27 mm)	35° (17.57 mm)	102.5° (15.28 mm)	198.1° (13.88 mm)	316.8° (3.71mm)	94.1° (15.44mm)	245.9° (12.96mm)	49.1° (16.76 mm)
Y_6=152.3mm	17.6° (19.53 mm)	17.6° (19.53 mm)	52.2° (16.6 mm)	118.9° (15 mm)	213.4° (13.62 mm)	331.1° (1 mm)	107.3° (15.19 mm)	258° (12.62 mm)	60.3° (16.32 mm)
Y_7=180.0mm	69.1° (16.03 mm)	69.1° (16.03 mm)	102.5° (15.28 mm)	166.9° (14.32 mm)	258.6° (12.6 mm)	13.1° (20.46 mm)	146.1° (14.61 mm)	293.9° (10.58 mm)	93.4° (15.45 mm)
Y_8=207.7mm	151.1° (14.54 mm)	151.1° (14.54 mm)	182.6° (14.11 mm)	243.7° (13.02 mm)	331.1° (1 mm)	80.9° (15.73 mm)	209.1° (13.7 mm)	352.3° (27 mm)	147.6° (14.59 mm)
Y_9=235.3mm	258.6° (12.6 mm)	258.6° (12.6 mm)	288° (11.12 mm)	345.2° (27 mm)	67.5° (16.08 mm)	171.6° (14.26 mm)	293.9° (10.58 mm)	71.4° (15.96 mm)	221.2° (13.48 mm)

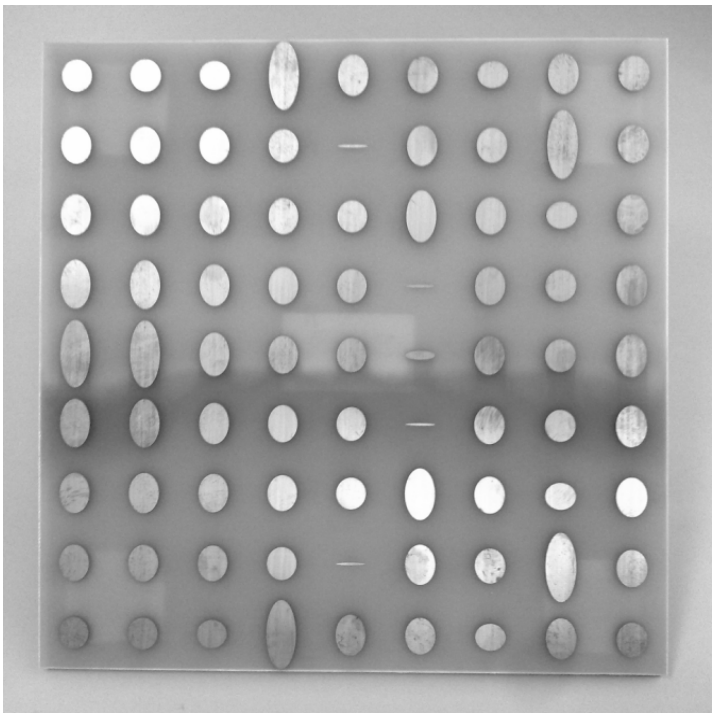

Figure 4.10: Photograph of fabricated elliptical patch reflectarray

The commercial pyramidal horn manufactured by ATM Inc. (Advance Technical Material) is used as the feeding source. Simulation of the horn is carried out to ascertain its performance. It has a dimension of 51.31mm (H) × 37.59mm (E), with a flare length F =73.5mm, as shown in Figure 4.11. Figure 4.12 (a) shows the simulated return loss of the horn antenna, which is more than -15 dB across the operating frequency range. The simulated radiation pattern of the horn antenna is shown in Figure 4.12 (b), giving a simulated antenna gain of 9.8 dBi (specification 10 dBi) and HPBW of 73.2^{o} at 6.5 GHz.

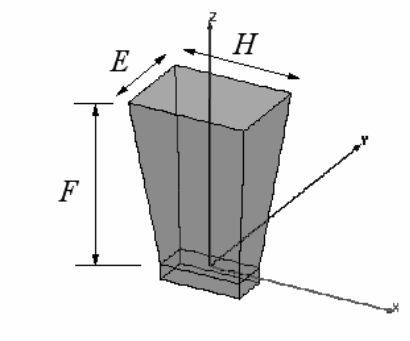

Figure 4.11: Simulation model of C-band feed horn.

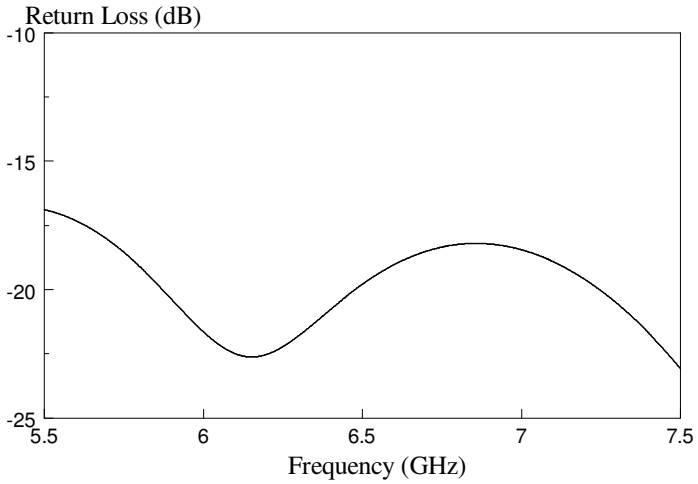

(a)

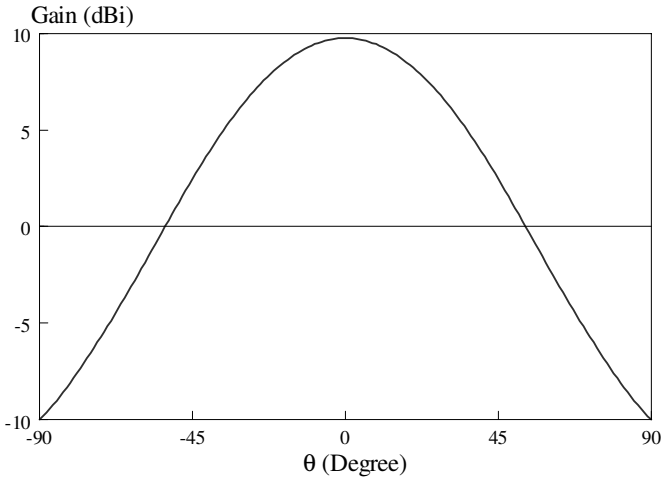

(b)

Figure 4.12: Simulated antenna characteristic of feed horn. (a) Return loss. (b) Radiation pattern

4.4.2.2 Circular Patch Reflectarray

With the use of (x_1, y_5) as the reference, the propagation phase difference of the corner element at (x_9, y_9) is again calculated as 221.2°. But now, the circular patch that is able to supply this additional phase has a radius of R = 6.78 mm. Other phases and their corresponding compensating patch radius are given in Table 4.3. The element sizes are used to build the simulation model shown in Figure 4.13, with the horn suspended at the same position. A photograph of the fabricated circular patch reflectarray is taken and illustrated in Figure 4.14.

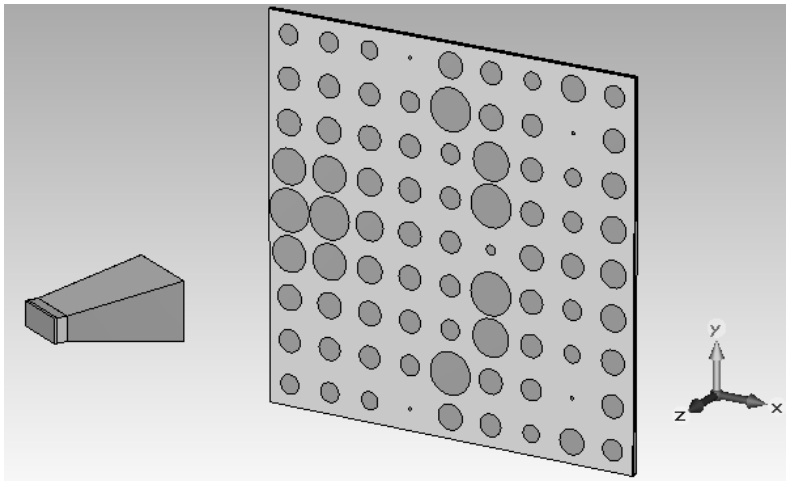

Figure 4.13: Simulation model of circular patch reflectarray.

Table 4.3: Additional phase shifts and the circular patch dimensions that are required to compensate the incident wave beams.

Phase difference, (Patch Size)	X_1=13.8mm	X_2=41.5mm	X_3=69.2mm	X_4=96.9mm	X_5= 124.6mm	X_6=152.3mm	X_7=180.0mm	X_8=207.7mm	X_9=235.3mm
Y_1=13.8mm	258.6° (6.35 mm)	258.6° (6.35 mm)	288° (5.72 mm)	345.2° (1 mm)	67.5° (8.23 mm)	171.6° (7.16 mm)	293.9° (5.5 mm)	71.4° (8.16 mm)	221.2° (6.78 mm)
Y_2=41.5mm	151.1° (7.31 mm)	151.1° (7.31 mm)	182.6° (7.08 mm)	243.7° (6.55 mm)	331.1° (13.7 mm)	80.9° (8 mm)	209.1° (6.88 mm)	352.3° (1 mm)	147.6° (7.33 mm)
Y_3=69.2mm	69.1° (8.21 mm)	69.1° (8.21 mm)	102.5° (7.73 mm)	166.9° (7.19 mm)	258.6° (6.36 mm)	13.1° (12.18 mm)	146.1° (7.35 mm)	293.9° (5.51 mm)	93.4° (7.83 mm)
Y_4=96.9mm	17.6° (11.52 mm)	17.6° (11.52 mm)	52.2° (8.62 mm)	118.9° (7.57 mm)	213.4° (6.84 mm)	331.1° (13.7 mm)	107.3° (7.68 mm)	258° (6.36 mm)	60.3° (8.39 mm)
Y_5=124.6mm	0° (13.7 mm)	0° (13.7 mm)	35° (9.43 mm)	102.5° (7.73 mm)	198.1° (6.97 mm)	316.8° (3.17 mm)	94.1° (7.82 mm)	245.9° (7.52 mm)	49.1° (8.72 mm)
Y_6=152.3mm	17.6° (11.52 mm)	17.6° (11.52 mm)	52.2° (8.62 mm)	118.9° (7.57 mm)	213.4° (6.84 mm)	331.1° (13.7 mm)	107.3° (7.68 mm)	258° (6.36 mm)	60.3° (8.39 mm)
Y_7=180.0mm	69.1° (8.21 mm)	69.1° (8.21 mm)	102.5° (7.73 mm)	166.9° (7.19 mm)	258.6° (6.36 mm)	13.1° (12.18 mm)	146.1° (7.35 mm)	293.9° (5.51 mm)	93.4° (7.83 mm)
Y_8=207.7mm	151.1° (7.31 mm)	151.1° (7.31 mm)	182.6° (7.08 mm)	243.7° (6.55 mm)	331.1° (13.7 mm)	80.9° (8 mm)	209.1° (6.88 mm)	352.3° (1 mm)	147.6° (7.33 mm)
Y_9=235.3mm	258.6° (6.35 mm)	258.6° (6.35 mm)	288° (5.72 mm)	345.2° (1 mm)	67.5° (8.23 mm)	171.6° (7.16 mm)	293.9° (5.5 mm)	71.4° (8.16 mm)	221.2° (6.78 mm)

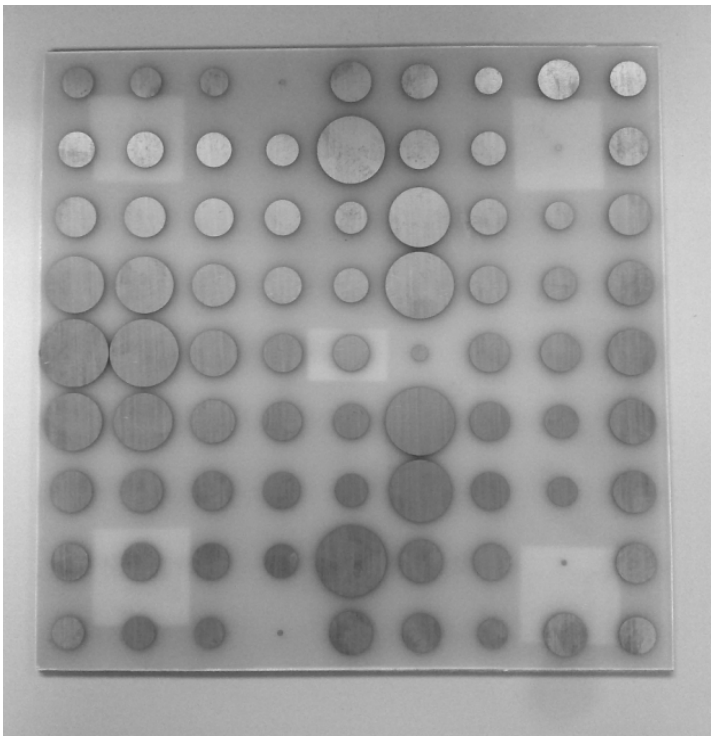

Figure 4.14: Photograph of fabricated circular patch reflectarray.

4.4.3 Simulation and Measurement

The commercial software CST Microwave Studio is used to simulate both the elliptical and circular reflectarray models shown in Figure 4.9 and 4.13. The accuracy limit is set to be -30 dB in the simulation. Further increasing the limit does not bring significant results improvement but increasing the simulation time. A high speed workstation Dell Precision T7500 (Intel (R) Xeon ® CPU with 24 GB RAM) coupled with the NVIDIA Tesla C2070 (GPU computing supported) is used for simulation.

4.5 Comparison of the Elliptical and Circular Reflectarrays

In this section the performances of the elliptical and circular patch reflectarrays are compared. Design parameters such as radiation patterns, 1-dB gain bandwidth, and HPBW are discussed.

4.5.1 Radiation Patterns

Figure 4.15 compares the simulated and measured radiation patterns in the *xz*-plane of the proposed elliptical and circular reflectarrays, for both the co- and cross-polarized fields. In the broadside direction ($\theta = 0^o$) of the reflectarray, the measured antenna gain reads 21.9 dBi (simulation 21.9 dBi) and 20.2 dBi (simulation 21.1 dBi) for the elliptical and circular cases, respectively. The HPBW of the elliptical reflectarray is 10.5^o and that for the circular one is 10.2^o. For both, the phase-shifting elements have successfully compensated all the incident wave beams, resulting in a directive plane wave in the boresight. Similar trend has been observed in the co- and cross-polarized radiation patterns in the *yz*-plane in Figure 4.16.

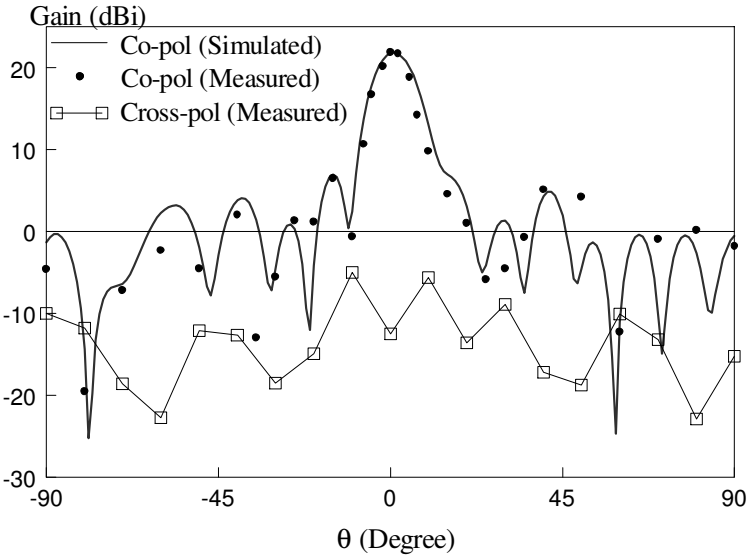

(a)

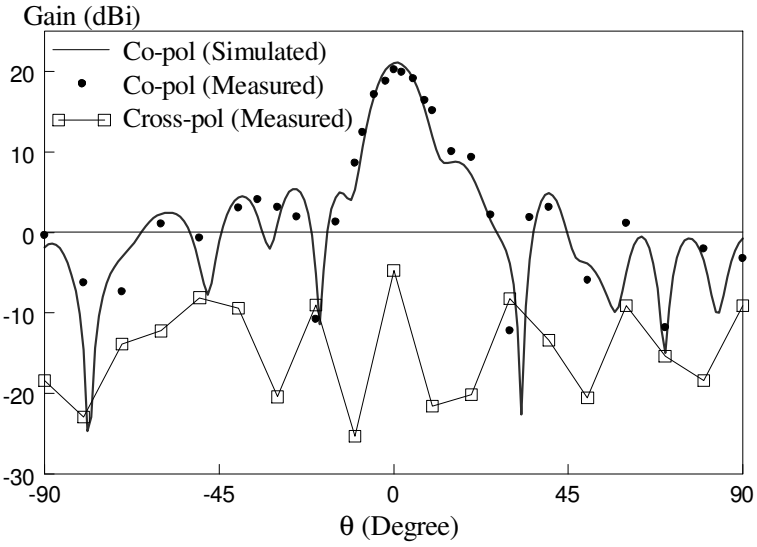

(b)

Figure 4.15: Comparison between the simulated and measured radiation patterns in the *xz*-plane. (a) Elliptical reflectarray. (b) Circular reflectarray.

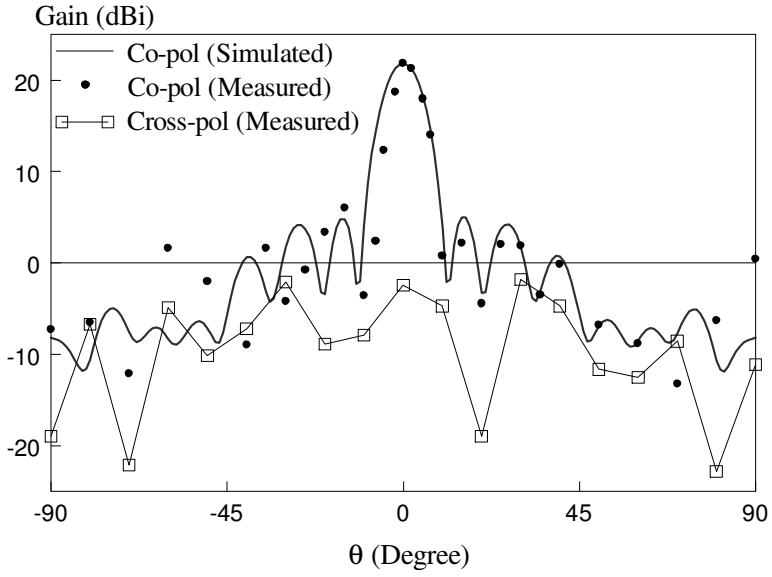

(a)

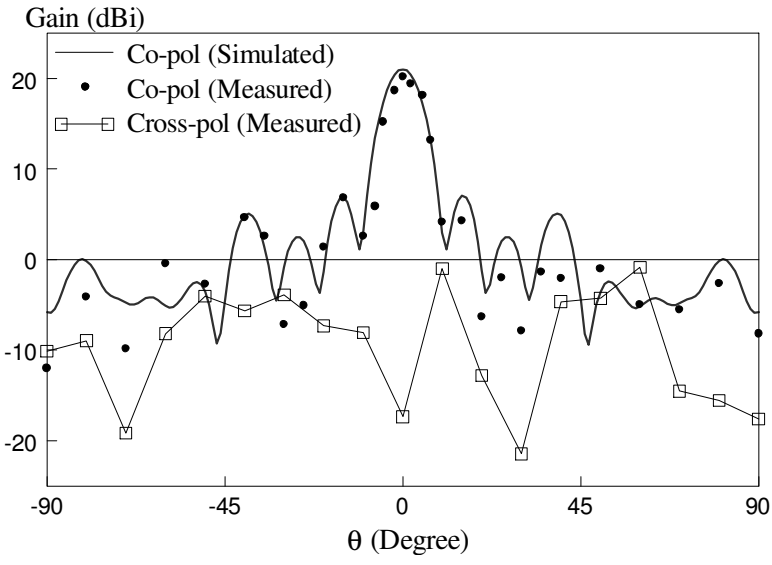

(b)

Figure 4.16: Comparison between the simulated and measured radiation patterns in the *yz*-plane. (a) Elliptical reflectarray. (b) Circular reflectarray.

4.5.2 1-dB Gain Bandwidth

For a reflectarray, the 1-dB gain bandwidth is used to describe the performance of the reflectarray when the operating frequency sways away from the center frequency. The frequency range in which the antenna gain is no less than 1dB from the maximum is defined as the 1-dB gain bandwidth of a reflectarray. The measurement method in Section 3.3 is used to measure the antenna gain of the reflectarray. Figure 4.17 shows the simulated and measured 1-dB gain bandwidths for the elliptical and circular reflectarrays. It is observed that the elliptical reflectarray has a measured 1-dB gain bandwidth of 11.08% (simulated = 12.3%), which is slightly larger than the 9.1% bandwidth (simulated = 9.6%) for the circular reflectarray.

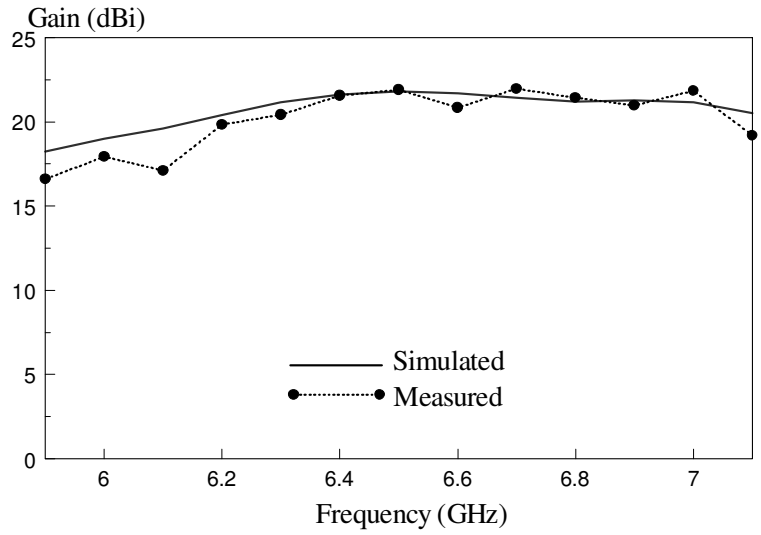

(a)

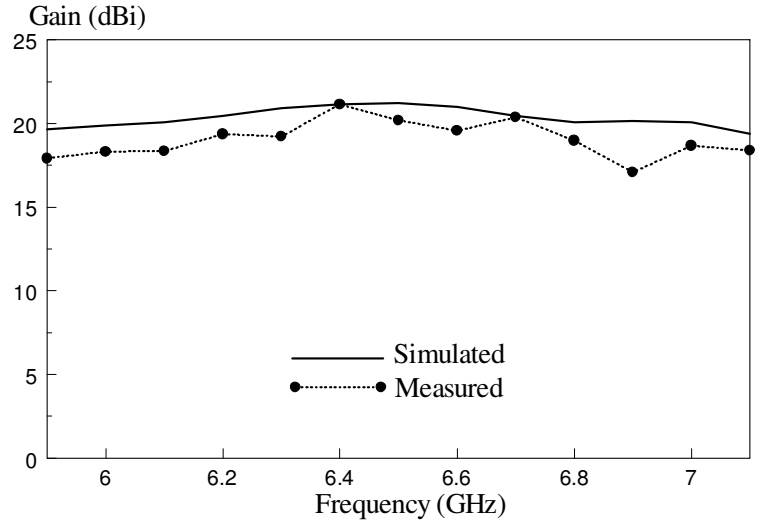

(b)

Figure 4.17: The 1-dB gain bandwidth as a function of frequency. (a) Elliptical patch reflectarray. (b) Circular patch reflectarray.

4.6 Parametric Analysis for Elliptical Patch Element

Parametric analysis has been carried out to examine the performance of the unit element of the elliptical reflectarray. Design parameters such as patch width, element spacing, air layer thickness, and operating frequency will be presented here.

4.6.1 Minor Width of Elliptical Patch

Although the width (*B*) in the minor axis is not as a phase-shifting dimension, it can slightly affect the reflection characteristics. Figure 4.18 shows the reflection loss and S-Curve with varying *B*. It is noted that the reflection loss decreases from -1.83dB to -1.01dB when the *B* is changed from *6* mm to 18 mm. This is due to the change of the patch resonance frequency. Rapid phase change is found around *A* = 14mm.

4.6.2 Element Spacing

The element spacing of the proposed elliptical patch reflectarray element is varied from 0.55 λ to 0.65 λ and the reflection characteristics are analyzed. This effect can be visualized by changing the cell dimension (*L*) of the unit cell. The simulation results are shown in Figure 4.19. It is obvious that the chosen element spacing is the most optimum to have both the broad phase range and slow gradient simultaneously.

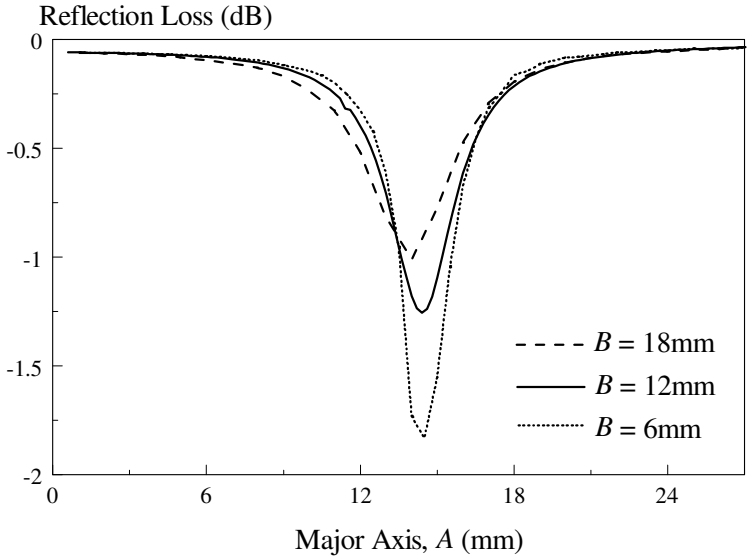

(a)

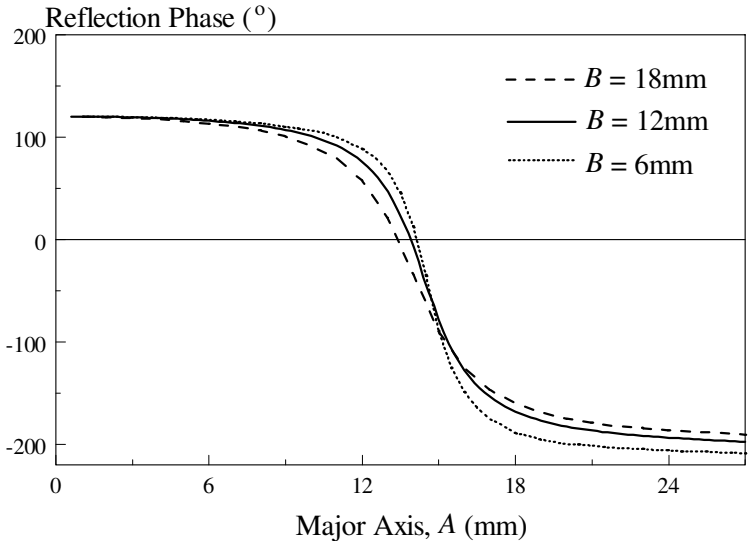

(b)

Figure 4.18: (a) Reflection loss and (b) S-Curve of the elliptical patch when its width *B* is varied.

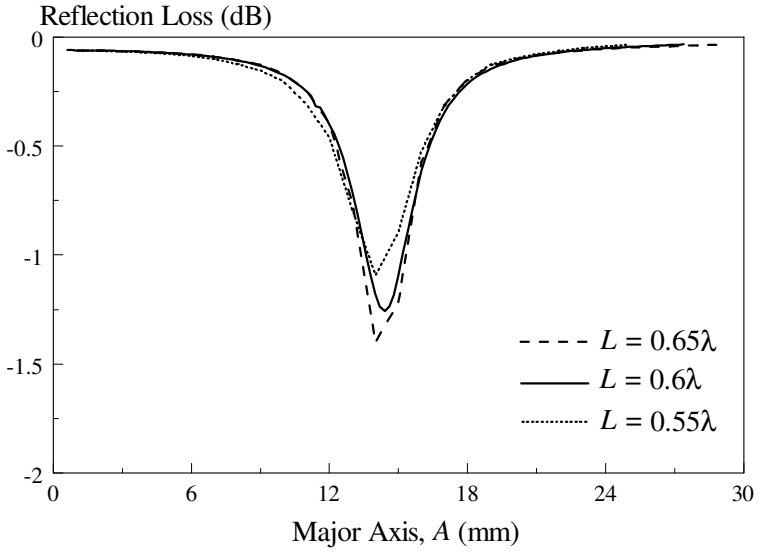

(a)

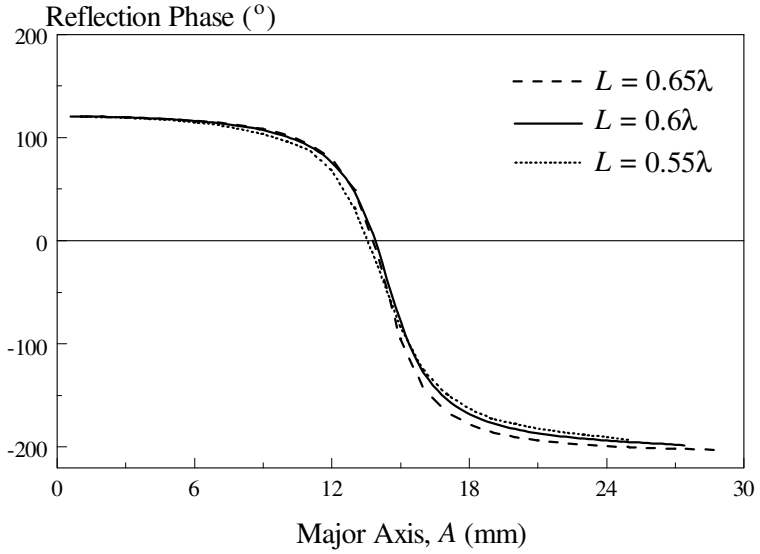

(b)

Figure 4.19: (a) Reflection loss (b) S-Curve of the elliptical reflectarray element for different element spacing.

4.6.3 Air Layer

Figure 4.20 shows how the reflection loss and S-Curve are affected by the air-layer thickness (h_2) between the substrate and ground plane. Small thickness causes the phase change to increase from 298.31° (h_2 = 3 mm) to 330° (h_2 = 1 mm), with the price of having steeper gradient and higher reflection loss, increasing from -0.9 dB to -1.99 dB. Thick air layer has low reflection loss but it reduces the phase changeable range significantly.

4.6.4 Frequency Performance

Figure 4.21 shows the reflection characteristics for different operating frequencies. When the operating frequency goes up, it is noted that smaller patch length (A in the major axis) is required to compensate the same phase difference. This is due to the reduction of operating wavelength. The maximum reflection loss remains around the same magnitude, but it is moving in the same trend as the operating wavelength.

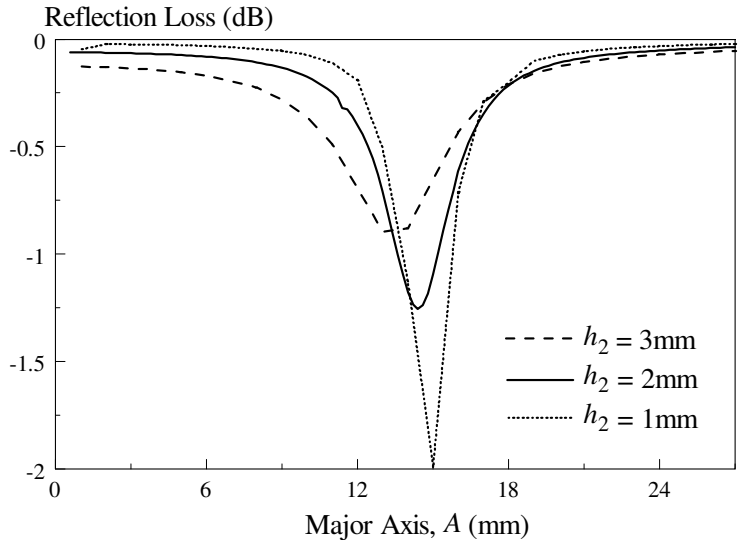

(a)

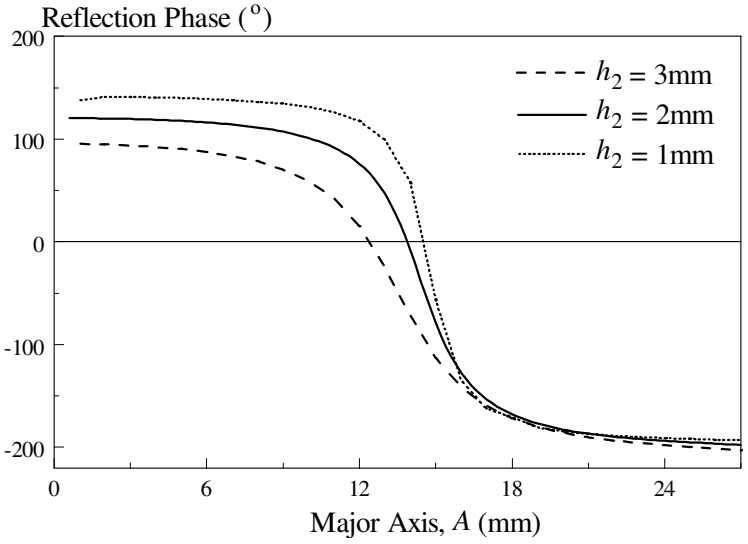

(b)

Figure 4.20: (a) Reflection loss and (b) S-Curve for different thicknesses of air layer.

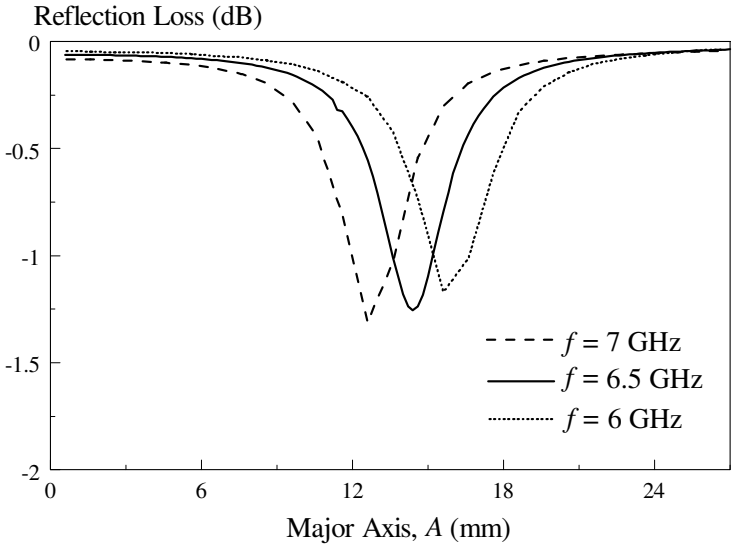

(a)

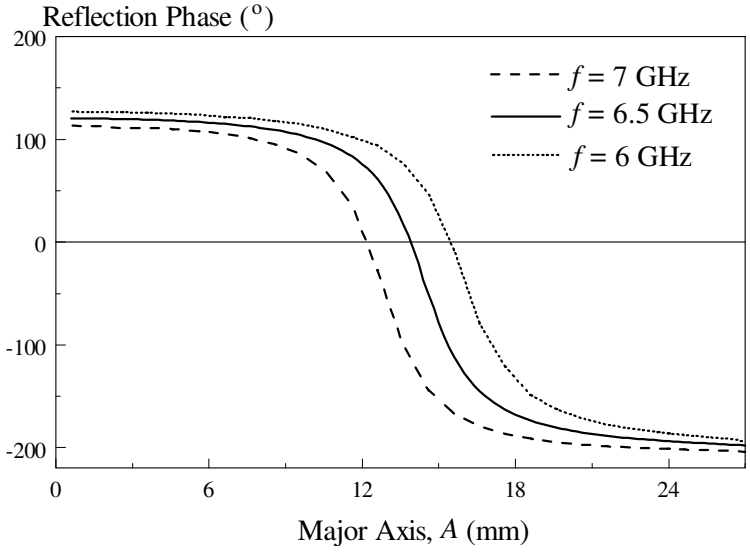

(b)

Figure 4.21: (a) Reflection loss and (b) S-Curve for the elliptical reflectarray when it is working at different frequencies.

4.7 Parametric Analysis for Circular Patch Element

In this section, parametric analysis has been performed on the key design parameters such as element spacing, air layer thickness, and operating frequency. The patch radius is now a phase-shifting dimension here.

4.7.1 Element Spacing

Again, as shown in Figure 4.22, the effect of the element spacing of the circular reflectarray is studied by changing the cell dimension (L) in the range of 0.55 λ - 0.65 λ. The simulation result shows that L = 0.6 λ gives broad phase range, along with a slow gradient.

4.7.2 Air Layer

The thickness of the air layer is varied and its effect is investigated. Figure 4.23 shows the simulated reflection loss and S-Curve as a function of the thickness. When h_2 is changed from 1 mm to 3 mm, the phase range decreases from 333.82^{o} to 304.93^{o}. Thicker air layer induces less loss.

4.7.3 Frequency Performance

With reference to Figure 4.24, again, smaller radius is needed to compensate the same phase at a higher operating frequency. This is reasonable due to the decrease in wavelength.

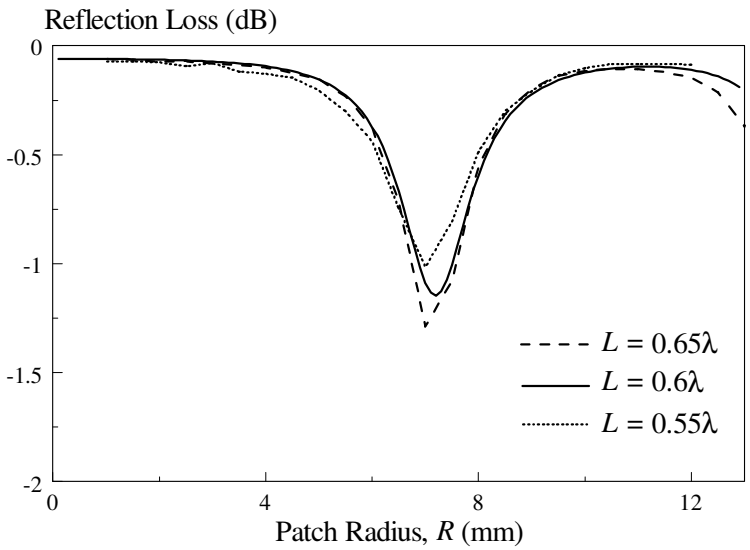

(a)

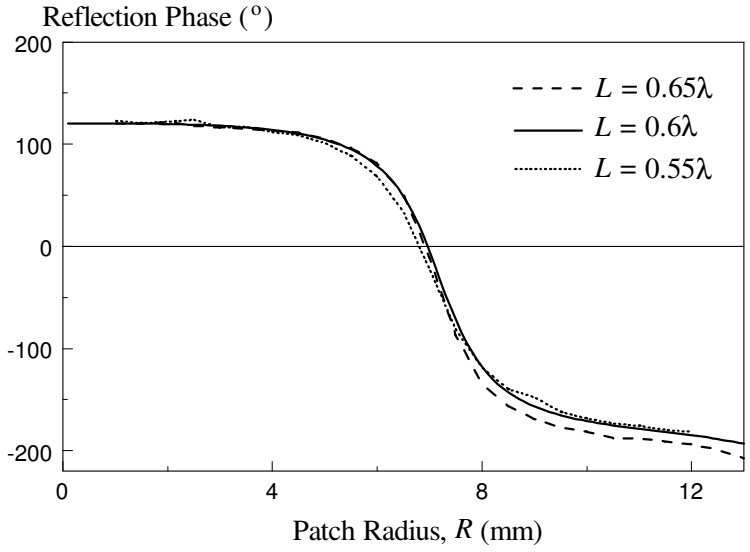

(b)

Figure 4.22: (a) Reflection loss (b) S-Curve of the circular reflectarray element for different element spacing.

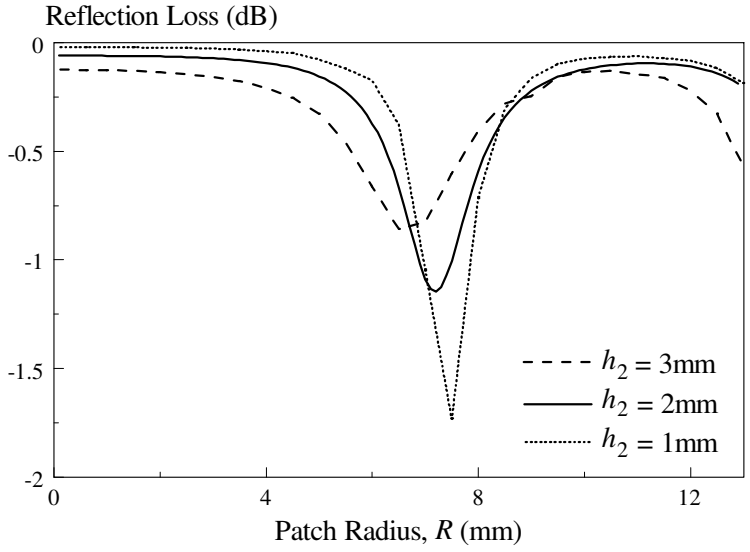

(a)

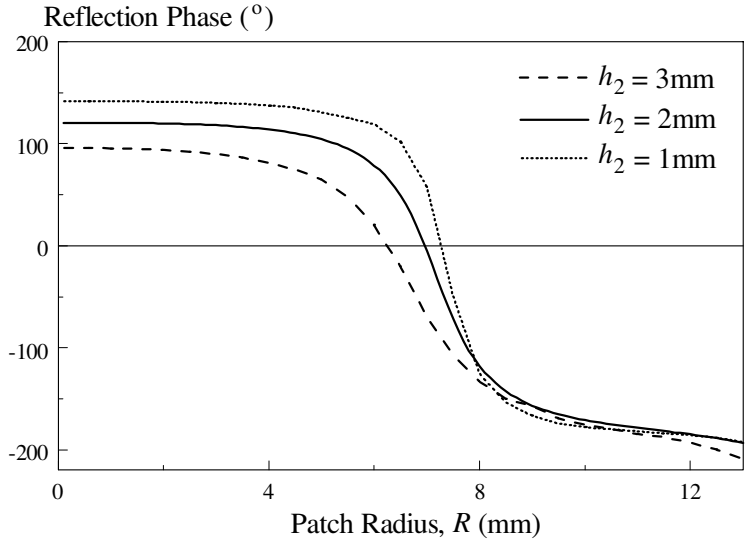

(b)

Figure 4.23: (a) Reflection loss and (b) S-Curve for different thicknesses of air layer.

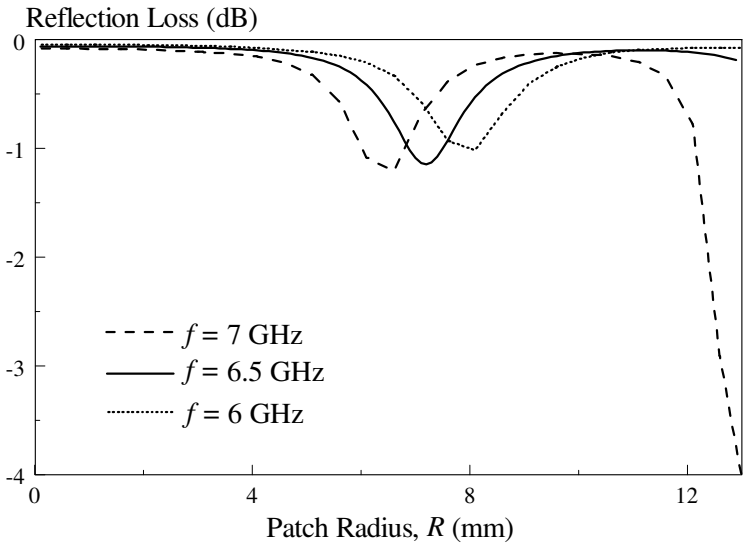

(a)

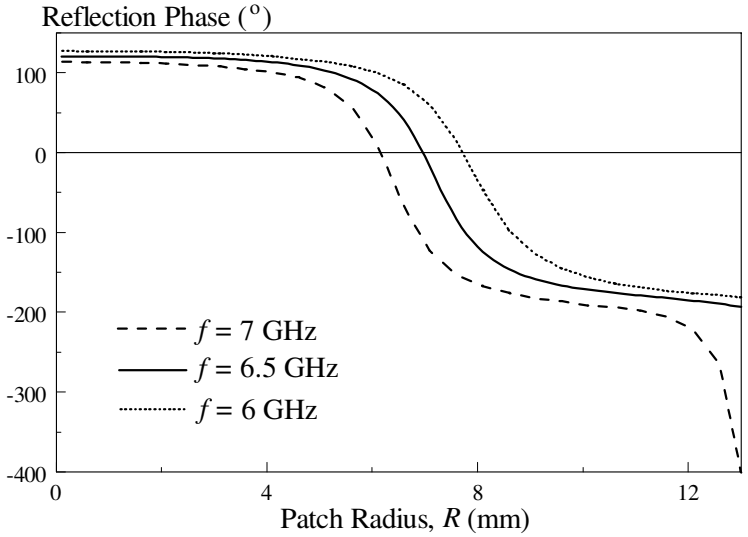

(b)

Figure 4.24: (a) Reflection loss and (b) S-Curve for the circular reflectarray when it is working at different frequencies.

4.8 Conclusions

The elliptical and circular microstrip patch reflectarrays are compared. Floquet method was used to design the reflectarray, verified with simulations and measurements. The use of foam-backed substrate is found to be able to improve the phase changing rate of the S-Curve, comparing with the single-layered one. This is useful for minimizing phase errors as the differences among the elements are now more distinguished. It was found that the elliptical patch reflectarray has broader antenna gain bandwidth (12.3%) than its circular counterpart.

CHAPTER 5

CONCLUSIONS

This dissertation has discussed the design procedures, simulations, prototypes fabrication, and measurements of some novel reflectarrays. In the first part, the DRA reflectarray has been explored and the design challenges have been studied. Underlaid loading strips with varied lengths are used to provide phase shifts to the radiating elements of the DRA reflectarray. In the second part, the elliptical and circular microstrip patches have been used as the radiating elements of the planar reflectarrays. It was shown that the elliptical patch reflectarray has a broader gain-bandwidth than the circular one. More interestingly, the use of the foam-backed substrate has been proven to be able to reduce the steepness of the S curve, which eases the fabrication process.

BIBLIOGRAPHY

1. Wong, H. Y., Lim, E. H. and Lo, F. L. A DRA reflectarray element with top-loading inclined strip. *Microwave and Optical Technology Lett*. (Submitted)

2. Wong, H. Y., Lim, E. H. and Lo, F. L. DRA reflectarray with underlaid metallic strip of variable length. *IEEE Trans. Antennas Propag.* (Submitted)

3. Wong, H. Y., Lim, E. H. and Lo, F. L. Elliptical and circular patch reflectarray on multi-layered substrate. *IEEE Trans. Antennas Propag.* (Submitted)

REFERENCES

Abd-Elhady, A. M. and Wei Hong, 2010. Ka-band linear polarized air vias reflectarray. *IEEE Middle East Conf. on Antennas and Propag*. (MECAP), pp. 1-3.

Abd-Elhady, A. M., Wei Hong and Zhang, Y., 2012. A Ka-band reflectarray implemented with a single-layer perforated dielectric substrate. *IEEE Antenna and Wireless Propagation Lett.*, 11, pp. 600-603.

Abd-Elhady, A. M., Zainud-Deen, S. H., Mitkees, A. A. and Kishk, A. A., 2010. X-band linear polarized aperture-coupled DRA reflectarray. *International Conf. on Microwave and Millimeter Wave Technology*, pp. 1042-1044.

Abd-Elhady, A. M., Zainud-Deen, S. H., Mitkees, A. A., and Kishk, A. A., 2012. Dual polarized dual feed aperture-coupled DRA reflectarray. *29th National Radio Science Conf. (NRSC)*, pp. 97-102.

Adel, S. and Hammad, H., 2013. A novel microstrip rotating cell for CP-reflectarray applications. *IEEE Radio and Wireless Symposium*, pp. 121-123.

Ahmadi, F., Forooraghi, K., Atlasbaf Z. and Virdee, B., 2013. Dual linear-polarized dielectric resonator reflectarray antenna. *IEEE Antennas Wireless Propag. Lett.*, 12, pp. 635–638.

Almajali, E., McNamara, D., Shaker, J. and Chaharmir, M. R., 2012. Derivation and validation of the basic design equations for symmetric subreflectarrays. *IEEE Trans. Antennas Propag.*, 60 (5), pp. 2336– 2346.

Alsath, M. G. N., Kanagasabai M. and Arunkumar, S., 2012. Dual-band dielectric resonator reflectarray for C/X-bands. *IEEE Antennas Wireless Propag. Lett.*, 11, pp. 1253–1256.

Arrebola, M., Encinar, J. A., Alvarez, Y., Las-Heras, F., 2006. Design and evaluation of a three-beam LMDS central station antenna using reflectarrays. *IEEE Mediterranean Electrotechnical Conf.*, pp.328-331.

Arrebola, M., Encinar, J. A. and Barba, M., 2008. Multifed printed reflectarray with three simultaneous shaped beams for LMDS central station antenna. *IEEE Trans. Antennas Propag.*, 56 (6), pp. 1518–1527.

Arrebola, M., Encinar, J. A., Fuente L. D. L. and Toso G., 2009. Contoured-beam reflectarray for DBS application including copolar isolation requirements between missions. *3rd European Conf. on Antennas and Propag*., pp. 844-848.

Berry, D., Malech, R. and Kennedy, W., 1963. The reflectarray antenna. *IEEE Trans. Antennas Propag*., AP-11 (6), pp. 645–651.

Biallowski M. E. and Encinar, J., 2007. Reflectarray: potential and challenges. *International Conf. on Electromagnetics in Advanced Applications* (ICEAA), pp. 1050-1053.

Bialkowski M. E. and Sayidmarie, K. H., 2008. Investigations into phase characteristics of a single-layer reflectarray employing patch or ring elements of variable size. *IEEE Trans. Antennas Propag.*, 56 (11), pp. 3366–3372.

Bialkowski, M. E., Song, H. J., Luk, K. M. and Chan, C. H., 2001. Theory of an active transmit/reflected array of patch antennas operating as a spatial power combiner. *IEEE Antennas and Propagation Society Int. Symp. Digest*, 4, pp. 764–767.

Boccia, L., Venneri, F., Angiulli, G., Amendola, G. and Massa, G. D., 2002. An experimental approach to active and passive reflectarray design. *32nd European Microwave Conf.,* pp. 1-4.

Bozzi, M., Germani, S. and Perregrini, L., 2004. A figure of merit for losses in printed reflectarray elements. *IEEE Antennas Wireless Propag. Lett.*, 3, pp. 257–260.

Budhu J. and Rahmat-Samii, Y., 2011. Understanding the appearance of specular reflection in offset fed reflectarray antennas. *Proc. IEEE AP-S Int. Symp. and USNC/URSI*, pp. 97–100.

Capozzoli, A., Curcio, C., D'Elia, G., Liseno, A., Bresciani, A. and Legay, D., 2009. Fast phase-only synthesis of faceted reflectarrays. *3rd Eur. Conf. Antennas and Propag*., pp. 1329-1333.

Capozzoli, A., Curcio, C., D'Elia, G., Liseno A. and Sparice, S., 2007. A design technique of reflectarrays with improved frequency performances. *2nd European Conf. on Antennas and Propag*., pp. 1-6.

Capozzoli, A., Curcio, C., D'Elia, G. and Liseno, A., 2010. Fast phase-only synthesis of conformal reflectarrays. *IET Microw. Antennas Propag*., 4 (12), pp. 1989–2000.

Capozzoli, A., Curcio, C., Liseno, A., Migliorelli M. and Toso, G., 2012. Phase-only synthesis of aperiodic reflectarrays with multi-frequency specifications. *IEEE Antennas and Propagation Society Int. Symp*., pp. 1-2.

Capozzoli, A., Curcio, C., Liseno, A., Migliorelli M. and Toso, G., 2012. Phase-only synthesis of conformal aperiodic reflectarrays with multi-frequency specifications. *6th European Conf. on Antennas and Propag*., pp. 2220-2224.

Carrasco, E., Arrebola M. and Encinar J. A., 2007. Shaped beam reflectarray using aperture-coupled delay lines for LMDS central station. *2nd European Conf. on Antennas and Propag*., pp. 1-6.

Carrasco, E., Arrebola, M., Encinar, J. A. and Barba, M., 2008. Demonstration of a shaped beam reflectarray using aperture-coupled delay lines for LMDS central station antenna. *IEEE Trans. Antennas Propag*., 56 (10), pp. 3103–3111.

Chang D.-C. and Huang, M.-C., 1992. Microstrip reflectarray antenna with offset feed. *Electronics Lett.*, 28 (16), pp. 1489-1491.

Chang D.-C. and Huang, M.-C., 1995. Multiple-polarization microstrip reflectarray antenna with high efficiency and low cross-polarization. *IEEE Transactions on Antennas and Propag*., 43 (8), pp. 829-834.

CST Computer Simulation Technology AG, Microwave Studio (MWS) [Online]. Available at: www.cst.com/Content/Products/MWS/Overview.aspx. [29 July 2013]

Dzulkipli, N. I., Jamaluddin, M. H., Yusof, M. F. M., 2012. Design of alphabet shaped slot-loaded dielectric resonator reflectarray antenna at 12 GHz. *IEEE Asia Pacific Conf. on Applied Electromagnetic*, pp. 334-337.

Encinar, J. A., 1999. Design of two-layer printed reflectarrays for bandwidth enhancement. *Proc. IEEE Antenna Propag. Symp*., pp. 1164–1167.

Encinar, J. A., 2001. Design of two-layer printed reflectarrays using patches of variable size. *IEEE Trans. Antennas Propag*., 49 (10), pp. 1403–1410.

Encinar, J. A., Arrebola, M., Fuente, L. D. L. and Toso, G., 2011. A transmit-receive reflectarray antenna for direct broadcast satellite applications. *IEEE Trans. Antennas Propag*., 59 (9), pp. 3255–3264.

Encinar, J. A., Datashvili, L. S., Zornoza, J. A., Arrebola, M., Castaner, M. S., Besada-Sanmartin, J. L., Baier, H. and Legay, H., 2006. Dual polarization dual-coverage reflectarray for space applications. *IEEE Trans. Antennas Propag.*, 54 (10), pp. 2827–2837.

Encinar J. A. and Zornoza, J. A., 2003. Broadband design of three-layer printed reflectarrays. *IEEE Trans. Antennas Propag*., 51 (7), pp. 1662–1664.

Encinar J. A. and Zornoza, J. A., 2004. Three-layer printed reflectarrays for contoured beam space applications. *IEEE Trans. Antennas Propag*., 52 (5), pp. 1138–1148.

Han C. and Chang, K., 2003. Ka-band reflectarray using ring elements. *Electron. Lett.*, 39, pp. 491–493.

Han, C., Huang, J. and Chang, K., 2006. Cassegrain offset subreflector-fed X/Ka dual-band reflectarray with thin membranes. *IEEE Trans. Antennas Propag.*, 54 (10), pp. 2838–2844.

Hasani, H., Kamyab, M. and Mirkamali, A., 2010. Broadband reflectarray antenna incorporating disk elements with attached phase-delay lines. *IEEE Antennas Wireless Propag. Lett.*, 9, pp. 156–158.

Hasani, H., Kamyab, M., Mirkamali A. and Eskandari, H., 2010. Reflectarray antenna consisting of circular disk elements: design and measurement. *Proc. Asia Pacific Microwave Conf.,* pp. 1565–1568.

Huang, J., 1991. Microstrip reflectarray. *Proc. Antennas and Propagation Society Int. Symp. Digest*, 2, pp. 612–615.

Huang, J., 1995. Analysis of a microstrip reflectarray antenna for microspacecraft applications. *TDA Progress Report 42-120*, pp. 153-173.

Huang, J., 1996. Capabilities of printed reflectarray antennas. *IEEE International Symposium on Phased Array Systems and Technology*, pp. 131-134.

Huang J. and Encinar, J. A., 2007. *Reflectarray antennas*. Hoboken, NJ: John Wiley & Sons.

Huang J. and Pogorzelski, R. J., 1997. Microstrip reflectarray with elements having variable rotation angles. *Proc. IEEE Int. Symp. Antennas Propag.*, 2, pp. 1280–1283.

Huang J. and Pogorzelski, R. J., 1998. A Ka-band microstrip reflectarray with elements having variable rotation angles. *IEEE Trans. Antennas Propag.*, 46, pp. 650–656.

Jamaluddin, M. H., Gillard, R., Sauleau, R., Coq, L. L., Castel, X., Benzerga R. and Koleck, T., 2009. A dielectric resonator antenna (DRA) reflectarray," *European Microwave Conf.*, pp. 025-028.

Jamaluddin, M. H., Gillard, R., Sauleau, R., Dumon, P. and Coq, L. L., 2008. A low loss reflectarray element based on a dielectric resonator antenna (DRA) with a parasitic strip. *Proc. IEEE Antennas Propag. Soc. Int. Symp.*, pp. 1-4.

Jamaluddin, M. H., Gillard, R., Sauleau, R., Dumon, P. and Coq, L. L., 2008. Reflectarray element based on strip-loaded dielectric resonator antenna. *Electron. Lett.*, 44 (11), pp. 664–665.

Jamaluddin, M. H., Gillard, R., Sauleau, R., Koleck T. and Castel, X., 2010. Dielectric resonator antenna reflectarray in Ka-band. *IEEE Antennas Propag. Society Int. Symp.*, pp. 1-4.

Javor, R. D., Wu, X. D. and Chang, K., 1995. Design and performance of a microstrip reflectarray antenna. *IEEE Trans. Antennas Propag*., 43, pp. 932–939.

Karnati, K., Ebadi, S. and Gong, X., 2011. Effect of dielectric thickness on phase swing of a Ka-band microstrip reflectarray unit cell. *Proc. IEEE Int. Symp. Antennas Propag., Dig*., pp. 948–951.

Karnati, K., Ebadi, S. and Gong, X., 2012. Effects of inter-element spacing on mutual coupling and resonant properties in reflectarray unit cell design. *IEEE Radio and Wireless Symposium*, pp. 83-86.

Karnati, K., Ebadi, S. and Gong, X., 2013. Dependency of Ka-band reflectarray unit cell reflection properties on the spacing between antenna elements. *IEEE Radio and Wireless Symposium*, pp. 118-120.

Karnati, K., Yusuf, Y., Ebadi, S. and Gong, X., 2013. Theoretical analysis on reflection properties of reflectarray unit cells using quality factors. *IEEE Trans. Antennas Propag*., 61 (1), pp. 201–210.

Keller, M. G., Shaker, J., Ittipiboon, A. and Anter, Y. M. M., 2000. A Ka-band dielectric resonator antenna reflectarray. *Proc. 30th Eur. Conf. Microw.*, pp. 272–275.

Makdissy, T., Gillard, R., Fourn, E., Girard E. and Legay, H., 2012. A patch-slot combination approach for large band reflectarrays. *42nd European Microwave Conf.,* pp. 759-762.

Mener, S., Gillard, R., Sauleau, R., Cheymol, C. and Potier, P., 2013. Design and characterization of a CPSS-based unit-cell for circularly polarized reflectarray applications. *IEEE Trans. Antennas Propagat*., 61 (4), pp. 2313-2318.

Milon, M. A., Gillard, R., Cadoret, D. and Legay, H., 2006. Comparison between the ‘infinite array’ approach and the ‘surrounded-element’ approach for the simulation of reflectarray antennas. *IEEE Antennas and Propagation Society Int. Symp*., pp. 4339-4342.

Munson, R. E., Haddad H. and Hanlen, J., 1987. Microstrip reflectarray for satellite communication and RCS enhancement or reduction. *US Patent* 4 684 952.

Mussetta, M., Grimaccia F. and Zich, R. E., 2012. Comparison of different optimization techniques in the design of electromagnetic devices. *IEEE Congress on Evolutionary Computation (CEC)*, pp. 1-6.

Mussetta, M., Pirinoli, P., Bliznyuk, N., Engheta, N. and Zich, R. E., 2006. Frequency response of a gangbuster surface off-set reflectarray antenna. *Proc. IEEE Antennas Propag. Soc. Int. Symp.*, pp. 4327–4330.

Mussetta, M., Zhang, W.X., Wang, A.N., Chen, H.H. and Zich, R.E., 2007. Frequency response optimization of a double layer reflectarray antenna. *IEEE Antennas and Propagat. Society Internatinal Sympos*., pp. 5319-5322.

Nayeri, P., Yang, F. and Elsherbeni1 A. Z., 2012. Design of single-feed reflectarrays with asymmetric multi-beams. *IEEE Antennas and Propag. Society Internatinal Sympos.*, pp. 1-2.

Niaz, M. W., Ahmed, Z. and Bin Ihsan, M., 2010. Performance comparison of different aperture shapes for microstrip reflectarray. *German Microwave Conf.*, pp. 250-253.

Pan, Y., Zhang Y. and Karimkashi S., 2012. Broadband low-cost reflectarray for multi-mission radar applications. *IEEE Radar Conf.*, pp. 0613-0617.

Pozar, D. M., 2003. Bandwidth of reflectarrays. *Electronics Letters*, 39 (21), pp. 1490-1491.

Pozar D. M. and Metzler, T. A., 1993. Analysis of a reflectarray antenna using microstrip patches of variable size. *Electron. Lett.*, 29 (8), pp. 657–658.

Pozar, D. M., Targonski, S. D. and Pokuls, R., 1999. A shaped-beam microstrip patch reflectarray. *IEEE Trans. Antennas Propag.*, 47 (7), pp. 1167–1173.

Pozar, D. M., Targonski, S. D. and Syrigos, H. D., 1997. Design of millimeter wave microstrip reflectarrays. *IEEE Trans. Antennas Propag.*, 45, pp. 287–296.

Rajagopalan H. and Rahmat-Samii, Y., 2010. On the reflection characteristics of a reflectarray element with low-loss and high-loss substrates. *IEEE Antennas Propag. Mag*., 52 (4), pp. 73–89.

Robinson, A. W., Bialkowski, M. E. and Song, H. J., 1999. An X-band passive reflect-array using dual-feed aperture-coupled patch antennas. *Proc. Asia Pacific Microwave Conf.*, 3, pp. 906–909.

Venneri, F., Costanzo, S. and Massa, G. D., 2008. Wideband aperture-coupled reflectarrays with reduced inter-element spacing. *Proc. IEEE Antennas Propag. Society Int. Symp.*, pp. 1-4.

Venneri, F., Costanzo, S. and Massa G. D., 2013. Design and validation of a reconfigurable single varactor-tuned reflectarray. *IEEE Trans. Antennas Propag.*, 61 (2), pp. 635-645.

Yang, F., Kim, Y., Yu, A., Huang, J. and Elsherbeni, A. Z., 2007. A single layer reflectarray antenna for C/X/Ka bands applications. *Int. Conf. on Electromagnetics in Advanced Applications*, pp. 1058–1061.

Yu, A., Yang, F., Elsherbeni, A. Z. and Huang, J., 2009. Design and measurement of a circularly polarized Ka-band reflectarray antenna. *Proc.3rd EuCAP*, pp. 2769–2773.

Zainud-Deen, S. H., Abd-Elhady, A. M., Mitkees, A. A., and Kishk, A. A., 2010. Dielectric resonator reflectarray with two DRA sizes and varying slot loading. *Proc. IEEE Antennas Propag. Soc. Int. Symp*., pp. 1-4.

Zhang, W. X., Fu, D. L. and Wang, A. N., 2007. A compound printed air-fed array antenna. *Proc. Int. Conf. Electromagn. Adv. Appl.*, pp. 1054–1057.

Zhao, M.-Y., Zhang, G.-Q., Lei, X., Wu, J.-M. and Shang, J.-Y., 2013. Design of new single-layer multiple-resonance broadband circularly polarized reflectarrays. *IEEE Antennas Wireless Propag. Lett.*, 12, pp. 356–359.

Zhou, M., Sørensen, S. B., Kim, O. S., Jørgensen, E., Meincke, P. and Breinbjerg, O., 2013. Direct optimization of printed reflectarrays for contoured beam satellite antenna applications. *IEEE Trans. Antennas Propag*., 61 (4), pp. 1995-2004.